The influence of the nonlinear behaviour of connecting bolts on the shear stiffness of circular joints in a tunnel segmental lining

Tunnelling and Underground Space Technology 146 (2024) 105619

Contents lists available at ScienceDirect

Tunnelling and Underground Space Technology incorporating Trenchless Technology Research

journal homepage: www.elsevier.com/locate/tust

The influence of the nonlinear behaviour of connecting bolts on the shear stiffness of circular joints in a tunnel segmental lining

Xin Han [a,b], Pierpaolo Oreste [b,*], Fei Ye [a]

[a] School of Highway, Chang'an University, Middle-Section of Nan'er Huan Road, Xi'an 710064, Shaanxi, China
[b] Department of Environment, Land and Infrastructure Engineering (DIATI), Politecnico di Torino, Corso Duca degli Abruzzi 24, 10129 Turin, Italy

ARTICLE INFO

Keywords:
Segmental Tunnel Lining
Circular Joint
Bolt connection of segments
Shear stiffness
FEM model
Winkler reaction spring

ABSTRACT

The segmental lining is a very common type of lining of tunnels, which is adopted when the TBM (Tunnel Boring Machine) is used as an excavation machine. It has a very important static task, because it has to support the loads transmitted by the ground or rock around the tunnel.

This segmental lining has a complex mechanical behaviour, conditioned by the presence of joints (circumferential and longitudinal ones) that exist between the different segments. The joints are connected to each other through different types of devices: the most used are steel bolts, which can be linear or curved.

In this paper, the mechanical behaviour of the circumferential joints has been studied in detail, in the presence of bolts to ensure the connection between the different rings of the lining. More specifically, the influence of the bolts on the shear stiffness of the joints was analysed; it has a fundamental role in the development of the stresses and displacements of the segmental lining along the tunnel axis.

To analyse the behaviour of the connecting bolts of the lining rings, specific numerical FEM models have been developed: they are able to evaluate the shear stiffness of the circumferential joint during the relative displacement between the rings facing the same circumferential joint.

Some practical applications referring to real cases have made it possible to detect which are the geometric and mechanical parameters of the bolts that have a greater role on the shear behaviour of the circumferential joint. The comparison of the results obtained from the developed numerical models with the measurements of the laboratory tests allowed to validate the numerical models.

Thanks to the achieved results, it is therefore now possible to define the characteristics of the connecting bolts of the segmental lining rings, also in relation to the possible consequences on the tensional and deformative state in the segmental lining and on the risk of damage due to possible high stress values in the concrete or in the steel constituting the bolts.

1. Introduction

When excavating a tunnel with Tunnel Boring Machines (TBMs), the precast concrete segmental lining is regularly inserted to support the ground around the tunnel. The lining is composed of segments along the circumferential and longitudinal direction, which are connected each other by bolts. The bolts can be divided into different types: straight bolt (parallel to the tunnel axial direction), curved bolt and inclined bolt (Fig. 1). Zhang et al. (2020b) collected the joint parameters of 32 TBM tunnels from China, and obtained some interesting results: inclined bolts are frequently adopted when the tunnel diameter is larger than 10m; otherwise, curved bolts or straight bolts are adopted. Feng et al. (2018) listed the joint structure of large diameter TBM tunnels which have been recently constructed in China: inclined bolts have been a typical type for segmental lining joints. Some cases of larger diameter tunnels (Zhang et al., 2020a) adopted the inclined bolt to connect the adjacent segmental rings, such as Yangtze River tunnel in Shanghai, China (2009), Weisan Road River Crossing Tunnel in Nanjing, China (2010), Qian River tunnel in Hangzhou, China (2014), 4th Elbe River Tunnel in Hamburg, Germany (2003). In these tunnels, the bolts alone bear the shear force on circumferential joints. More commonly, tenons are used together with bolts for the same aim. Based on the test and numerical results of Guo et al. (2023), the ultimate bearing capacity of the shear force for a joint can reduce, with reference to the case of the

* Corresponding author.
E-mail addresses: hanxin@chd.edu.cn (X. Han), pierpaolo.oreste@polito.it (P. Oreste), xianyefei@126.com (F. Ye).

https://doi.org/10.1016/j.tust.2024.105619
Received 21 June 2023; Received in revised form 11 January 2024; Accepted 22 January 2024
Available online 28 February 2024

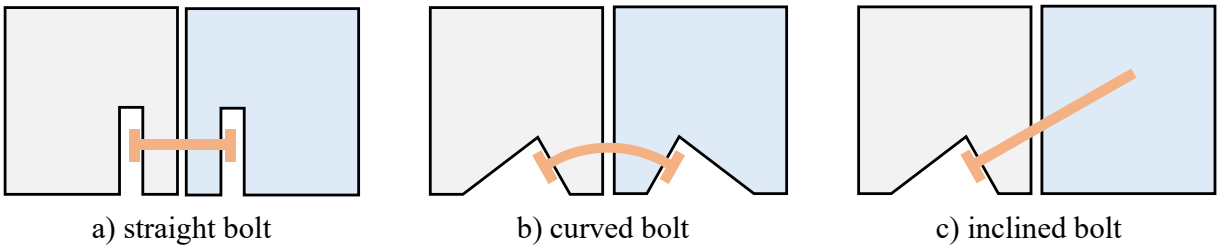

Fig. 1. The types of bolts which are generally adopted to connect segments along a circular joint in a tunnel segmental lining (after Han et al. (2023b)).

contemporary presence of tenons and bolts, to the 78.25 % (with only tenons and without bolts) and to the 45.92 % (with only bolts and without tenons). It means that both bolts and tenons have an important function for bearing the shear force on a joint.

The role of the bolts is even more important when a one component material is used to fill the gap between the segmental lining and the tunnel wall: in these cases, a large distance of the lined tunnel starting from the TBM tail has a fluid material (during its maturation and before its setting) surrounding the segment rings and the lining buoyancy phenomenon can cause high shear forces, which have to be absorbed by the devices mentioned above (bolts and tenons) in order to avoid serious damages to the concrete structure inside the tunnel.

In other fields of geomechanical and structural engineering, bolts are frequently adopted to reinforce rock joints and concrete joints (Chen et al., 2020; Li et al., 2021; Nie et al., 2020; Oreste and Spagnoli, 2021; Oreste and Cravero, 2008).

Because the stiffness of the circular joint is weaker than the lining ring, an important transversal displacement and stress concentration can be found around the joint along the tunnel axial direction under the application of the grouting pressure, the jack thrust, the ground load, the uneven settlement of the ground, etc. (Chen and Mo, 2009; Feng et al., 2022; Huang et al., 2018; Xu et al., 2019; Yang et al., 2017). The characteristics of the bending deformation, the shear deformation and the crack development of the circular joint were analysed based on laboratory tests (Ding et al., 2021; Feng et al., 2018; Li et al., 2019; Qiu et al., 2021; Zuo et al., 2022). Liu et al., (2021a) investigated the dislocation between the segmental lining rings, and found that the high value of the dislocation leads to a large increasement of the settlement along the tunnel axis and also a great shear stress in the circular joints; furthermore, the concrete spalling can be observed in the zones with a large dislocation between the segmental lining rings (Liu et al., 2020). In order to reduce and avoid any damage of the segmental structure, it is important to evaluate the segmental lining deformation and the distribution of the internal forces and moments along the axial (longitudinal) direction of the tunnel, where the stiffness of the circular joints is a critical parameter for the correctness of the calculation results.

When calculating the tunnel deformation along the longitudinal direction using the numerical model, the lining structures including the segments, tenons and bolts are simulated by a simplified model of the real structure (Chaipanna and Jongpradist, 2019; Liu et al., 2021b; Shi et al., 2016; Shi et al., 2022). In this way, some details of the joint are usually not considered in order to save the memory and improve the calculating speed, which reduces the accuracy of the calculation results. Liu et al., (2021a) adopted the axial spring and the radial spring to represent the tensile stiffness and the shear one when analysing the tunnel deformation along the longitudinal direction and showing a good agreement with test results. In the theoretical solutions, the bending stiffness and the shear stiffnesses are critical parameters (Cheng et al., 2021; Geng et al., 2019; Liao et al., 2008; Wu et al., 2015). So it is very important to be able to determine both the bending stiffness and the shear stiffness of the circular joint for calculating the tunnel deformation along the longitudinal direction and the stress state inside the segmental lining using numerical models and also theoretical solutions. Among the stiffnesses of the circular joint, the bending stiffness has been more studied (Shiba et al., 1988; Cheng et al., 2021; Geng et al., 2019; Li et al., 2019; Liao et al., 2008; Shi et al., 2022; Shiba et al., 1988; Wu et al., 2015).

The shear stiffness of the joint is included into the model when the Timoshenko beam is adopted to analyse the deformation of the segmental lining along the tunnel longitudinal direction (Wu et al., 2015). Wu et al. (2015) proposed the equation of the equivalent shear stiffness which combined the shear deformations of the lining ring and of the joint, where the joint shear deformation only depends on the bolts' characteristics, and the influences of the tenon and the friction on the joint surfaces were neglected. Cheng et al. (2021) considered the three phases of the shear deformation with the relative displacement of the adjacent segments on the circular joint: an initial friction phase, the bolt-hole wall gap closing phase, bolt and tenon bearing phase, where the shear stiffness at the friction phases is neglected, while the shear stiffness $(kGA)_s$ during the gap closing phase, the one of bolt $(n \bullet k_b G_b A_b)$ and that of the tenon $(k_g G_g A_g)$ are introduced to calculate the equivalent shear stiffness of the segmental lining. Han et al., (2023a) developed a shear stiffness equation as a ratio between the ultimate shear force of the joint, which can be obtained by the bolt shear strength, and the maximum relative displacement, which considers the influence of the gap between the bolt and the hole wall together with the bolt shear deformation. On these developed models, the shear stiffness of the circular joint is calculated based on the shear stiffness of the bolt, and it is considered as a constant value or with different constant values for each different phase.

The shear deformation of the bolt and of the tenon on the joint is not only influenced by their own deformation, but also by that of the surrounding concrete. The shear stiffness of the joint always develops following a nonlinear curve as the relative displacement varies; it means that the joint shear law follows a nonlinear behaviour. Furthermore, Feng et al. (2018) and Zuo et al. (2022) pointed out that the failure of the joint is due to the obvious cracks on the concrete. The joint behaviour shows an elasto-plastic behaviour due to the yielding of the bolt and the development of cracks on the concrete hole wall where the bolt is inserted. Considering the influence of the concrete hole wall, Han et al., (2023c) simulated the reaction of the hole wall by normal springs which are applied along the bolt axis; they developed a calculation procedure to determine the shear stiffness of the joint based on a simplified cantilever beam theory. However, the influence of the constraints on the bolt head by the concrete and the screw nut on the bolt deformation and then on the joint shear deformation was not fully considered.

For the nonlinear behaviour of the joint shear law (shear force vs. transversal relative displacement of the lining rings), there are two main reasons: structural nonlinearity and material nonlinearity. Regarding the structure of the joint, there is a gap between the bolt and the bolt hole, and the bolt movement related to the bolt hole will cause the closure of the gap and then it leads to a compressive reaction of the concrete on the hole wall to the bolt. On the other hand, during the compressive deformation of both the bolt and the bolt hole, the steel and concrete materials will have initially an elastic behaviour and then a plastic one: the stiffness of the joint will decrease when the materials tends to yield. At the end of the plastic phase, the limit state for the steel and concrete affects the maximum achievable joint deformation. In this

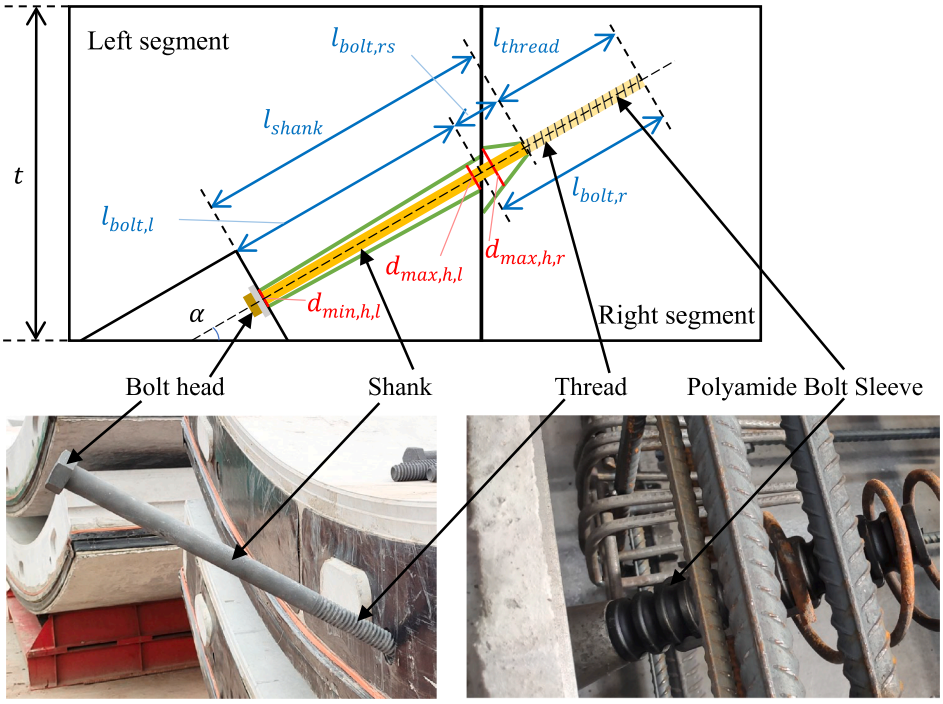

Fig. 2. The typical structure of an inclined bolt crossing a circular joint.

Table 1
Key parameters of segmental joints and inclined bolts in different real cases of China.

No.	D_e(m)	t(mm)	*Joint type*	d_b(mm)	α(°)	Left segment			Right segment			Reference
						$d_{min,h,l}$(mm)	$d_{max,h,l}$(mm)	$l_{bolt,l}$(mm)	$d_{max,h,r}$(mm)	$l_{bolt,rs}$(mm)	l_{thread}(mm)	
1	15	650	Circ	M36	34	42	52	465	/	81.2	200	(Zhang et al., 2020a)
2	15	650	Long	M36	35	42	52	465	/	80	200	
3	15.4	650	Circ	M36	/	42	52	465	68	80	220	(Zhang et al., 2022)
4	11.8	500	Circ	M30	30	36	46	368	/	60	160	(He et al., 2021)
5	14.5	600	Circ	M36	/	42	/	470	/	80	190	(Guo et al., 2011)
6	15	650	Circ	M30	30	/	/	530	/	60	/	(Li et al., 2011)
7	11.6	550	Long	M40	30	46	54	403.5	/	70	220	(Geng et al., 2020)

paper only the nonlinear behaviour due to the structure of the joint is analysed; this affects the first phase of the joint deformation, when the materials have an elastic behaviour. Therefore, an elastic behaviour of the joint materials is assumed in the following.

In order to analyse this nonlinear characteristic in detail, a new numerical model was developed based on the Timoshenko beam theory and Finite Element Method (FEM) and proposed in this paper. By this model, the nonlinear behaviour of the joint can be studied comprehensively, including the deformation of the bolt and the internal forces developed along the axial direction. Furthermore, the shear stiffness of the joint can be evaluated as the relative displacement of the segments varies. Based on the obtained calculation results the critical characteristics of the constraints type at the bolt head can be found, and some simplified analytic solutions can be determined. Therefore, useful simplified equations of the joint shear stiffness can be obtained.

Thanks to the developed numerical model for the joint shear deformation, the influence of the bolt and the concrete on the joint shear stiffness can be quickly evaluated, including the bolt diameter, the bolt length, the bolt strength, the diameter of the bolt hole, the strength of the concrete on the bolt hole, the pre-tensile force inside the bolt; also, the nonlinear behaviour of the joint shear deformation can be obtained. The obtained simplified equation of the joint shear stiffness can be then used in the modelling of the segmental lining in numerical models in order to analyse the tunnel lining deformation and the state of stress in the concrete segments and on the circular joints, along the axial direction.

2. Analysis of the behaviour of the bolt under a relative transversal movement between lining rings

2.1. Bolt shear deformation under relative displacements of concrete portions

The typical scheme of the joint with an inclined bolt inserted in two different segments is shown on Fig. 2. The inclined angle of the bolt with respect to the tangential direction is α. The bolt on the left segment is a shank which has a length $l_{bolt,l}$, and is constrained by the bolt head and the washer. The bolt on the right segment with a length $l_{bolt,r}$ includes a shank part and a thread part, which have a length $l_{bolt,rs}$ and l_{thread} respectively; the thread part is connected to the concrete by a polyamide bolt sleeve. The total shank section of bolt is l_{shank}, and the total length of bolt is L ($L = l_{shank} + l_{thread}$). The values of the typical joint parameters

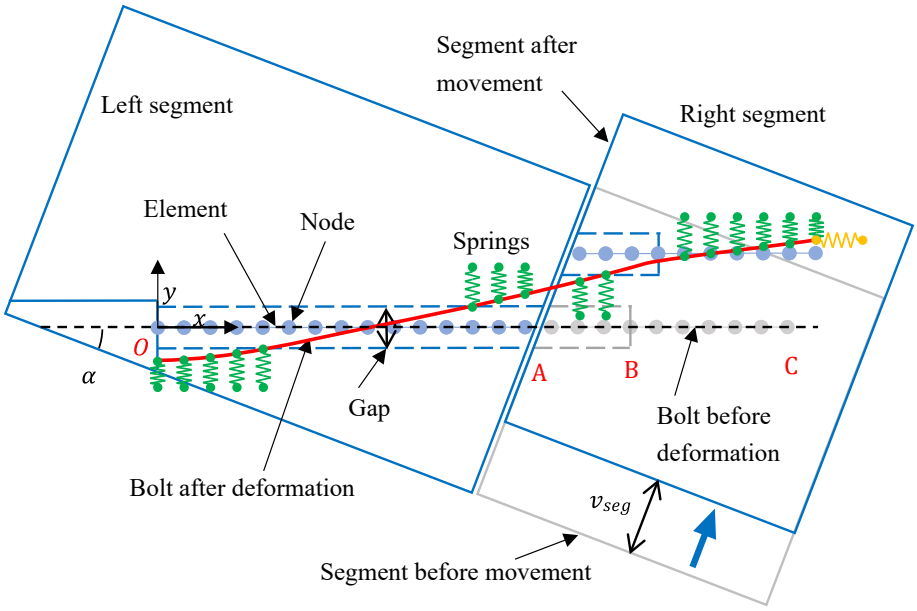

Fig. 3. The deformation of the inclined bolt when the adjacent segments have a relative displacement parallel to the joint. Where the v_{seg} is the relative displacement of the adjacent segments along the joint, *O* represents the bolt head and the first node on the bolt, *A* is the location of the joint, *B* is the point of intersection between the shank section of the bolt and the thread section, and *C* means the endpoint of the bolt.

for an inclined bolt are listed in Table.1 obtained from different real cases from China.

where D_e is the external diameter of the tunnel lining, t is the thickness of the lining, *Joint type* is the type of joint which includes the circumferential joint (Circ) and the longitudinal one (Long), d_b is the bolt diameter, $d_{max,h,l}$ is the maximum diameter of the bolt hole on the left segment, $d_{min,h,l}$ is the minimum diameter of the bolt hole on the left segment, $d_{max,h,r}$ is the maximum diameter of the bolt hole on the right segment.

When the segments have a relative displacement, the schematic diagram of the deformations and of the applied forces on the inclined bolt are shown in Fig. 3, and the deformation and the load are not symmetrical along the bolt. The model of the whole length bolt is adopted based on the coordinate system $(x-y)$, where the x-axis is represented by the bolt axial direction. On the section *OB* of the bolt (Fig. 3), a perpendicular compressive force can be applied on the bolt when the transversal bolt displacement is larger than the gap between the bolt and the bolt hole; on the section *BC*, a perpendicular compressive force and a parallel shear force at each node are applied on the bolt when the bolt has a relative displacement with the concrete (the shear spring is only shown at the last node of Fig. 3).

For the generic i element of the bolt, a balancing equation can be obtained:

$$[f]_{ex,i} + [f]_{in,i} = [k_b]_i \bullet [d]_i \tag{1}$$

where $[f]_{ex,i}$ is the external load vector on the two nodes of the element i, $[f]_{in,i}$ is the internal load vector on the two nodes of element i, $[d]_i$ is the displacement vector of the two nodes of element i, $[k_b]_i$ is the local stiffness matrix of element i. Because there are three freedom at each node $[x_i \quad y_i \quad \phi_i]$, the load vector and the displacement vector include 6 items, where i is the node number (the element i include the node i and node $i+1$, with $i = 1, 2, \cdots, n$).

By the Timoshenko beam theory, the local stiffness matrix $[k_b]_i$ of the element i is:

$$[k_b]_i = \begin{bmatrix}
\frac{EA_b}{l} & 0 & 0 & -\frac{EA_b}{l} & 0 & 0 \\
0 & \frac{12}{1+\Phi}\bullet\frac{EI}{l^3} & \frac{6}{1+\Phi}\bullet\frac{EI}{l^2} & 0 & -\frac{12}{1+\Phi}\bullet\frac{EI}{l^3} & \frac{6}{1+\Phi}\bullet\frac{EI}{l^2} \\
0 & \frac{6}{1+\Phi}\bullet\frac{EI}{l^2} & \frac{4+\Phi}{1+\Phi}\bullet\frac{EI}{l} & 0 & -\frac{6}{1+\Phi}\bullet\frac{EI}{l^2} & \frac{2-\Phi}{1+\Phi}\bullet\frac{EI}{l} \\
-\frac{EA_b}{l} & 0 & 0 & \frac{EA_b}{l} & 0 & 0 \\
0 & -\frac{12}{1+\Phi}\bullet\frac{EI}{l^3} & -\frac{6}{1+\Phi}\bullet\frac{EI}{l^2} & 0 & \frac{12}{1+\Phi}\bullet\frac{EI}{l^3} & -\frac{6}{1+\Phi}\bullet\frac{EI}{l^2} \\
0 & \frac{6}{1+\Phi}\bullet\frac{EI}{l^2} & \frac{2-\Phi}{1+\Phi}\bullet\frac{EI}{l} & 0 & -\frac{6}{1+\Phi}\bullet\frac{EI}{l^2} & \frac{4+\Phi}{1+\Phi}\bullet\frac{EI}{l}
\end{bmatrix} \tag{2}$$

where E is the elastic modulus of the bolt, A_b is the area of the bolt cross section, l is the length of the element i, I is the inertia moment of the bolt, Φ is the ratio between the bending stiffness (EI) and the shear stiffness (kGA_b) of the bolt, k is the shear coefficient based on the Timoshenko beam theory, and is equal to $k = 6(1+\nu_{st})/(7+6\nu_{st})$ (Cowper, 1966)), G is the shear elastic modulus of the bolt, and is equal to $G = E/(2(1+\nu_{st}))$, ν_{st} is the Poisson's ratio of bolt.

The stiffness matrix $[k_b]_i$ can be expressed by 4 submatrices:

$$[k_b]_i = \begin{bmatrix} \boldsymbol{k}_{i,i} & \boldsymbol{k}_{i,a} \\ \boldsymbol{k}_{i,b} & \boldsymbol{k}_{i,i+1} \end{bmatrix} \tag{3}$$

where $\boldsymbol{k}_{i,a}$ is the first 3×3 submatrix of the stiffness matrix $[k_b]_i$ along the sub diagonal, and is equal to the transpose of the submatrix $\boldsymbol{k}_{i,b}$; $\boldsymbol{k}_{i,i}$ is the first 3×3 submatrix at node i of element i along the major diagonal, and is equal to the following equation:

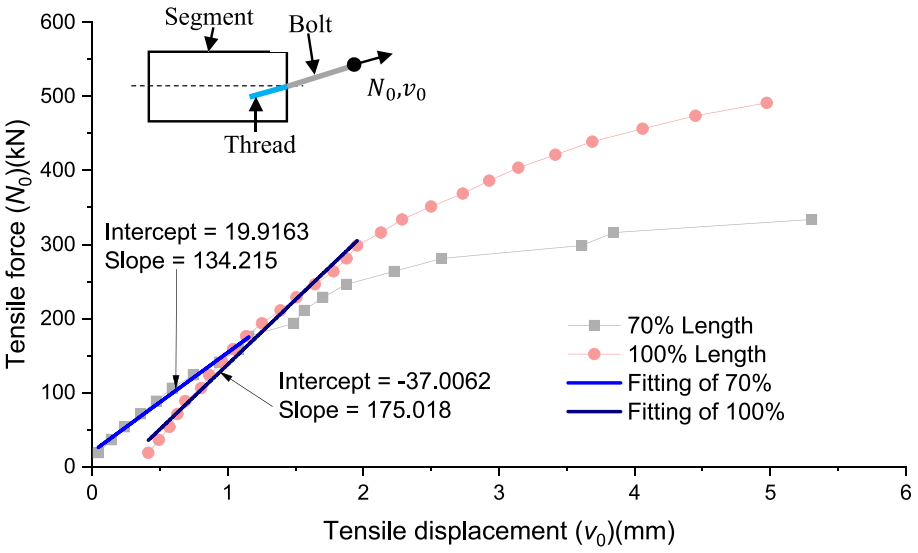

Fig. 4. The fitting analysis of the elastic deformation of the bolt based on the laboratory tests of Geng et al. (2020).

$$\boldsymbol{k}_{i,i} = \begin{bmatrix} \frac{EA_b}{l} & 0 & 0 \\ 0 & \frac{12}{1+\Phi} \bullet \frac{EI}{l^3} & \frac{6}{1+\Phi} \bullet \frac{EI}{l^2} \\ 0 & \frac{6}{1+\Phi} \bullet \frac{EI}{l^2} & \frac{4+\Phi}{1+\Phi} \bullet \frac{EI}{l} \end{bmatrix} \tag{4}$$

$\boldsymbol{k}_{i,i+1}$ is the last 3×3 submatrix at node $(i+1)$ of element i along the major diagonal.

$$\boldsymbol{k}_{i,i+1} = \begin{bmatrix} \frac{EA_b}{l} & 0 & 0 \\ 0 & \frac{12}{1+\Phi} \bullet \frac{EI}{l^3} & -\frac{6}{1+\Phi} \bullet \frac{EI}{l^2} \\ 0 & -\frac{6}{1+\Phi} \bullet \frac{EI}{l^2} & \frac{4+\Phi}{1+\Phi} \bullet \frac{EI}{l} \end{bmatrix} \tag{5}$$

Furthermore, the balancing equation of the whole bolt on the global coordinate system can be obtained:

$$[F] = [K] \bullet [D] \tag{6}$$

where the global matrix $[K]$ can be obtained by adding all the submatrix with the same node number along the main diagonal.

$$[K] = \begin{bmatrix} \boldsymbol{k}_{1,1} & \boldsymbol{k}_{1,a} & 0 & 0 & \cdots & 0 & 0 \\ \boldsymbol{k}_{1,b} & \boldsymbol{k}_{1,2} + \boldsymbol{k}_{2,2} & \boldsymbol{k}_{2,a} & 0 & \cdots & 0 & 0 \\ 0 & \boldsymbol{k}_{2,b} & \boldsymbol{k}_{2,3} + \boldsymbol{k}_{3,3} & \boldsymbol{k}_{3,a} & \cdots & 0 & 0 \\ 0 & 0 & \boldsymbol{k}_{3,b} & \boldsymbol{k}_{3,4} + \boldsymbol{k}_{4,4} & \cdots & 0 & 0 \\ \vdots & \vdots & \vdots & \vdots & \ddots & 0 & 0 \\ 0 & 0 & 0 & 0 & \cdots & \boldsymbol{k}_{n-1,n} + \boldsymbol{k}_{n,n} & \boldsymbol{k}_{n,a} \\ 0 & 0 & 0 & 0 & \cdots & \boldsymbol{k}_{n,b} & \boldsymbol{k}_{n,n+1} \end{bmatrix} \tag{7}$$

The external force vector $[F]$ includes the external load vector on each node $\boldsymbol{F}_i$ $(i = 1, 2, 3, \cdots, n+1)$, $[F] = [\boldsymbol{F}_1 \quad \boldsymbol{F}_2 \quad \cdots \quad \boldsymbol{F}_{n+1}]^T$, $\boldsymbol{F}_i = [F_{X,i} \quad F_{Y,i} \quad F_{\Phi,i}]^T$.

The displacements vector $[D]$ is constituted by the displacement vectors at each node $\boldsymbol{D}_i$, $[D] = [\boldsymbol{D}_1 \quad \boldsymbol{D}_2 \quad \cdots \quad \boldsymbol{D}_{n+1}]^T$, $\boldsymbol{D}_i = [D_{X,i} \quad D_{Y,i} \quad D_{\Phi,i}]^T$.

2.2. The additional terms considering the concrete compressive forces and the segments relative transversal displacements

(1) The normal reaction force of the concrete hole wall.

When the bolt compresses the concrete hole wall, a reaction force is applied on the bolt, and is equal to the normal displacement multiplied by the compressive stiffness of the concrete hole wall. The compressive stiffness matrix $\boldsymbol{K}_{r,i}$ as an additional term is added to the global matrix $[K]$ along the major diagonal.

$$\boldsymbol{K}_{r,i} = \begin{bmatrix} 0 & 0 & 0 \\ 0 & K_{r,i} & 0 \\ 0 & 0 & 0 \end{bmatrix} \tag{8}$$

where $K_{r,i}$ is the compressive stiffness of the hole wall on the local coordinate system, which can be obtained by the following equation:

$$K_{r,i} = k_c \bullet l_{av,i} \bullet d_b \tag{9}$$

where $l_{av,i}$ is the average length of the element around the i th node; k_c is the concrete foundation compressive modulus; and Soroushian et al., (1987b) suggested the following equation to calculate the concrete foundation compressive modulus:

$$k_c = \frac{127 \bullet f_{cc}^{0.5}}{(d_b)^{\frac{2}{3}}} \tag{10}$$

where f_{cc} is the uniaxial compressive strength of concrete.

The concrete foundation compressive modulus represents the entity of the reaction force between the bolt and the concrete hole wall, and is determined by the materials properties of the bolt and concrete. In addition, there is an obvious size effect when the bolt is compressed on the concrete due to the small diameter of the bolt. Limited test results are available and great differences can be found among them (Poli et al., 1992; Soroushian et al., 1987a; Yin et al., 2022); for this reason the suggested value by Eq.10 is adopted in the following to calculate the concrete foundation compressive modulus.

Before the movement of the bolt in the bolt hole in each point along the axial direction, there is a existing gap between the bolt and the hole wall, but the value of the gaps $d_{gap,i}$ of each point are different, as shown in Fig. 2. When the bolt transversal displacement $d_{y,i}$ is smaller than the existing gap $d_{gap,i}$, the bolt is not at contact with the concrete hole wall, and there are not any reaction forces; otherwise, an additional force $\boldsymbol{F}_{r,i} = [0 \quad F_{rY,i} \quad 0]^T$ is added to the external force $\boldsymbol{F}_i$ term based on the

Table 2
The parameters calculation based on the slope of the fitting lines and by using Eq.14 and Eq.15 for the 2 studied cases.

No.	Length of bolt on the concrete hole (l_{thread}: m)	Length of bolt out of the hole (l_{shank}: m)	Slop of the test results ($K_{s,t}$: MN/m)	Parameter (ρ: 1/m)	Concrete foundation shear modulus (β_c: MN/m^3)
1	0.154	0.546	134.125	2.207	10034.21
2	0.22	0.48	175.108	2.215	10110.49

compressive stiffness of the concrete hole wall.

$$F_{rY,i} = K_{r,i} \bullet d_{gap,i}/2 \tag{11}$$

(2) The shear reaction force of the concrete hole wall

Due to the friction force between the thread and the concrete which wraps the polyamide bolt sleeve, it applies a shear force on the bolt. The thread part of the bolt has a significant influence on the joint deformation.

On the thread part of the bolt, the shear force from the concrete can be obtained considering the existing shear stiffness and the developed relative displacement parallel to the bolt axis. The shear stiffness matrix $\boldsymbol{K}_{s,i}$ is an additional term in the global matrix $[K]$ along the major diagonal, and it can be obtained by the following equation:

$$\boldsymbol{K}_{s,i} = \begin{bmatrix} K_{s,i} & 0 & 0 \\ 0 & 0 & 0 \\ 0 & 0 & 0 \end{bmatrix} \tag{12}$$

where $K_{s,i}$ represents the applied shear force on each element of the bolt from the concrete hole wall, when the bolt has a unit length of relative displacement with the concrete hole wall; it is the shear stiffness and it can be obtained by the following equation:

$$K_{s,i} = \beta_c \bullet \pi \bullet d_b \bullet l_e \tag{13}$$

where β_c represent the shear stress when the bolt has an unitary relative displacement; it can be called concrete foundation shear modulus equal to $\beta_c = \tau/v$, where τ is the shear stress, and v is the relative displacement parallel to the bolt axis.

The value of β_c can be evaluated by the tensile test of a bolt installed in a concrete hole:

$$\beta_c = \frac{\rho^2 \bullet E \bullet d_b}{4} \tag{14}$$

where ρ is a parameter that can be obtained by the tensile stiffness $K_{s,t}$:

$$K_{s,t} = \frac{N_0}{v_0} = \frac{E \bullet A_b}{\frac{\coth(\rho \bullet l_{thread})}{\rho} + l_{shank}} \tag{15}$$

where N_0 is the applied tensile axial force, v_0 is the measured axial displacement of the bolt head. The detailed derivation of Eq.14 and Eq.15 are added to the Appendix. A.

Geng et al. (2020) analysed the stresses and the deformations of an inclined test bolt along the bolt axial direction (the parameters of the used bolts can be found in Table.1, No.7). The tensile displacement as the tensile force varies is shown in Fig. 4, which includes two different situations: the installed length of the thread part of the bolt is equal to 70 % of the total length of the thread part (case 1), and to 100 percent of the total length (case 2). For case 1, the length parameter l_{thread} is equal to 70 % of the true length on the thread section of bolt, and the length parameter l_{shank} is equal to the 30 % of the true value of the thread section plus the length of the shank section.

In Fig. 4, two different phases of the curves of the two cases can be seen. At the first phase, the tensile displacement linearly increases with the tensile force (the elastic phase); then, the increasement of the tensile displacement becomes larger with the increase of the tensile force. It means that the constraint force applied from the concrete hole to the bolt weakens with the increase of the tensile force. For the elastic stage, linear lines are used to fit the test results (Fig. 4). The parameter ρ and the concrete foundation shear modulus β_c can be calculated by using Eq.14 and Eq.15 based on the slope of the fitting lines, and the results are listed in Table.2.

Based on its definition, the concrete foundation shear modulus β_c is not influenced by the diameter of the bolt, but by the structure of the thread, the strength of the concrete hole wall, the polyamide bolt sleeve and the bolt itself. Adopting the same tensile test as the one of Geng et al. (2020), Eq.14 and Eq.15 can be used to calculate the concrete foundation shear modulus of the bolt hole for the elastic stage.

(3) The compressed force at the endpoint of the bolt.

Due to the constraints of the washer and the nut on the bolt head, there are tensile forces on the bolt when the segments have a relative displacement along the joint plane; these tensile forces can be calculated by knowing the concrete foundation compressive modulus and the type of constraint at the bolt head. The compressed stiffness of the concrete surface under the washer at the bolt head $K_{x,o}$ can be obtained by the following equation:

$$K_{x,o} = k_c \bullet \frac{\pi}{4} \bullet \left(d_{washer}^2 - d_h^2\right) \tag{16}$$

where d_{washer} is the diameter of the washer, d_h is the diameter of the bolt hole.

The following equation $\boldsymbol{K}_{\boldsymbol{X},o}$ need to be added to the matrix $\boldsymbol{k}_{1,1}$ of the global matrix $[K]$ in Eq.7.

$$\boldsymbol{K}_{\boldsymbol{X},o} = \begin{bmatrix} K_{x,o} & 0 & 0 \\ 0 & 0 & 0 \\ 0 & 0 & 0 \end{bmatrix} \tag{17}$$

Furthermore, the pre-tensile force $F_{p,x}$ on the endpoint O can be inserted in the system when a compressive reaction force is applied to the concrete segments over a joint.

2.3. The shear stiffness of the joint

Because the length of the zone of bolt-hole wall contact is not constant as the relative displacement increases, the shear stiffness of the joint varies and shows a nonlinear behaviour with the relative displacement. Generally, the average shear stiffness of the joint can be represented by the ratio between the shear force of the joint and the relative displacement together with the length of the joint element, which can be considered as the projection length of bolt L_{bp}:

$$(k \bullet G \bullet A)_{eq} = \frac{V_{total}}{v_{seg}} \bullet L_{bp} \tag{18}$$

where V_{total} is the shear force when the adjacent segments have a relative displacement v_{seg}, and can be obtained by the following equation:

$$V_{total} = V_{fric} + V_{bolt} + V_{tenon} \tag{19}$$

where the V_{tenon} is the component of the shear force on the joint due to the shear deformation of tenon, and the component V_{fric} from the friction depends on the compressed force and the friction angle:

$$V_{fric} = N \bullet \tan\left(\varphi_{joint}\right) \tag{20}$$

where φ_{joint} is the friction angle of the joint, N is the normal force applied on the joint.

The component of the shear force due to the bolt V_{bolt} can be obtained

Table 3
The constraint types considered on the endpoint O of the bolt (bolt head).

Case No.	Axial direction	Transversal direction	Rotation	Pre-tensile force	Sign
1	0	0	0	0	x = 0, y = 0, r = 0 (C1)
2	$K_{x,o}$	0	0	$0/F_p$	x = K, y = 0, r = 0 (C2)
3	$K_{x,o}$	Free	0	$0/F_p$	x = K, y free, r = 0 (C3)
4	$K_{x,o}$	Free	Free	$0/F_p$	x = K, y & r free (C4)

based on the shear and the normal forces on the joint:

$$V_{bolt} = Q_A \bullet \cos(\alpha) + N_A \bullet \sin(\alpha) \tag{21}$$

where Q_A is the shear force in the bolt on the joint A, and the N_A is the normal force in the bolt on the joint A.

The shear force on the joint due to the bolt deformation is analysed in the detail in this paper.

The ratio between the increasement of the shear force and the one of the relative displacement of the segments can be defined as an equivalent stiffness, which is a instantaneous joint shear stiffness without considering the length of the joint element K_{eq}:

$$K_{eq} = \frac{\Delta V_{total}}{\Delta v_{seg}} \tag{22}$$

When only considering the influence of the bolt deformation, the equivalent stiffness can be rewritten as the following equation based on Eq.21.

$$K_{eq} = K_{eq,Q} \bullet \cos^2(\alpha) + K_{eq,N} \bullet \sin^2(\alpha) \tag{23}$$

where $K_{eq,Q}$ is the shear stiffness of the bolt, which reprensents the instantaneous joint shear stiffness with straigth bolt (Fig. 1), and $K_{eq,N}$ is the tensile stiffness of the bolt, which reprensents the instantaneous joint tensile stiffness with straigth bolt. The two stiffnesses can be calculated by the following equations:

$$K_{eq,Q} = \frac{\Delta Q_A}{\Delta v_{s,y}} \tag{24}$$

$$K_{eq,N} = \frac{\Delta N_A}{\Delta v_{s,x}} \tag{25}$$

where $\Delta v_{s,y}$ is a component of the relative displacement of the segmental lining on the joint along y-axis on Fig. 3, $\Delta v_{s,y} = \Delta v_{seg} \bullet \cos(\alpha)$, and $\Delta v_{s,x}$ is a component along x-axis, $\Delta v_{s,x} = \Delta v_{seg} \bullet \sin(\alpha)$.

$K_{eq,Q}$ and $K_{eq,N}$ represent, respectively, the shear and tensile deformation performance of the joint when the joint is perpendicular to the bolt axial direction.

3. The inclined bolt behaviour

(1) The influence of the types of constraint of the bolt head on the bolt deformation

The changeability of the constraint on the bolt leads to a nonlinear behaviour of the joint. For the bolt body, the constraint from the hole wall is applied on the bolt as a compressed force and a shear force, which can be obtained based on the Part (1) and (2) of Sect.2.2. No constraint is present on the ending point C. The nut and the washer on the bolt head (point O) restrict the rotation and the transversal displacement to a certain degree in that point. In addition, the concrete will produce a reaction compressive force on the washer when the bolt is stretched due to the bolt deformation and/or the axial pretension. The concrete reaction force can be obtained by the Part (3) of Sect.2.2. Therefore, the combination of the constraints on the bolt head (Table.3) is discussed based on different conditions for the transversal displacement and the rotation: free or prevented; furthermore, the constraint in the axial direction refers to a pretension force present or absent.

In order to investigate the influence of the constraints on the bolt head, the gap between the bolt and the hole wall was considered constant; the key parameters which are adopted to analysis the bolt deformation in this section are listed in Table 4. In addition, the elastic modulus and the Passion's ratio of the bolt steel are 20600 MPa and 0.3, respectively; the ones of concrete are 34500 MPa and 0.167, respectively. The adopted value of the concrete foundation compressive modulus is 66.3 MPa/mm obtained by the Eq.10; the concrete foundation shear modulus on the thread part of the bolt is equal to 10.1 MPa/mm based on the test results of Geng et al. (2020).

In order to be able to analyse the influence of the constraint types on the bolt head, the relative displacement of segments of 5 mm and 10 mm are considered on the joint: the displacement components along the y-axis are 4.33 mm and 8.66 mm, and the one along the x-axis are 2.5 mm and 5 mm, due to the inclination of the bolt with respect to the joint. Based on the model of Fig. 3, the vertical displacement, the shear force, the rotation, the moment, the axial displacement and the axial force are calculated and shown in Fig. 5 to Fig. 10, where (C1-5) means that the case C1 is calculated for a 5 mm relative displacement of segments along the joint.

When the adjacent segments have a relative displacement along the joint, the bolt which is installed on the segments has an accompanying displacement. The transversal displacements of the bolt show an increasing trend from the endpoint O to the endpoint C, and the increasements of the transversal displacements near the joint A are larger than the ones near the endpoints. From Fig. 5, the constraints on the endpoint O has a great influence on the bolt deformation of the OA section and a weak influence on the AC section; the constraint along the axial direction does not affect the transversal displacement. When the segments have a small relative displacement (5 mm), the transversal displacement near the endpoint O is positive when the transversal displacement is free and the rotation is prevented; the transversal displacements are negative when the rotation is free. However, the transversal displacements are negative when there is a great relative displacement (10 mm for cases C3 and C4).

On Fig. 6, the maximum positive shear forces can be found on the thread section (BC), and the negative ones reach the maximum value at the joint A. When there is a small relative displacement, the bolt hole on the left segment near the joint is compressed; this leads to an increase of the shear force in the bolt. With the increase of the relative displacement, the bolt contacts with the hole wall, but the compressed zone of the hole wall on the left segment near the joint has a small increase. It is worth noting that the shear force tends to 0 near the point B, where the

Table 4
The key parameters adopted to evaluate the inclined bolt shear deformation.

d_b(mm)	α(°)	Left segment			Right segment		
		$d_{min,h,l}$(mm)	$d_{max,h,l}$(mm)	$l_{bolt,l}$(mm)	$d_{max,h,r}$(mm)	$l_{bolt,rs}$(mm)	l_{thread}(mm)
M36	30	42	42	465	42	80	200

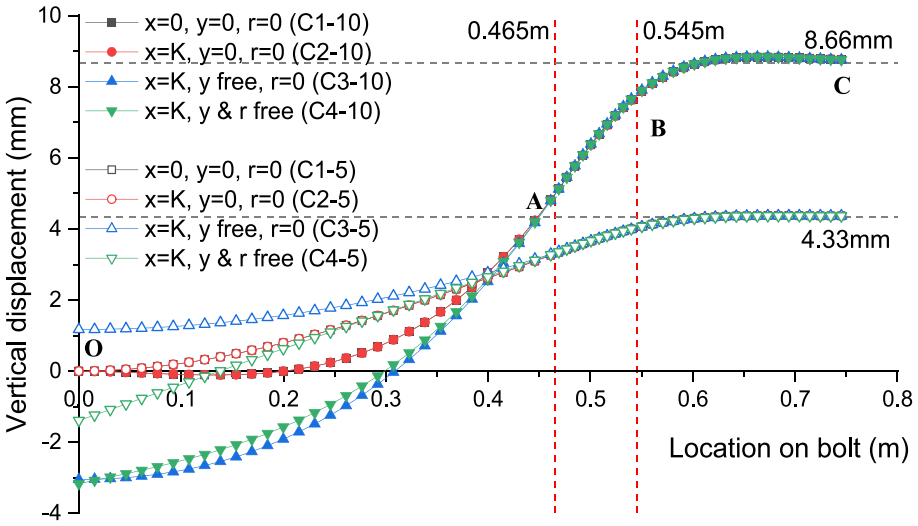

Fig. 5. Calculated transversal displacements along the bolt.

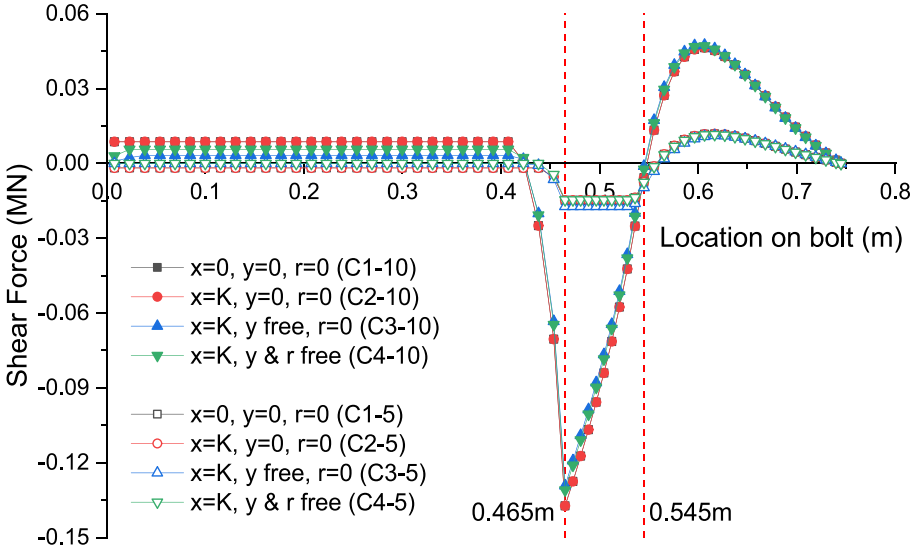

Fig. 6. Calculated shear forces along the bolt.

thread part of the bolt on the right segment starts. From Fig. 6 it is possible to note that the constraints on the endpoint *O* have a slight influence on the shear force of the bolt on the section *OB*.

On Fig. 7, the rotations of the bolt show an increasing trend on the *OA* section and a decreasing trend on the *AC* section; the maximum value is reached at the joint *A*. Furthermore, the constraints on the endpoint *O* have a significant influence on the bolt rotation on the *OA* section; the axial force on the endpoint *O* (pre-tension force) does not influence the rotation of the bolt. When the relative displacement is small (5 mm), the rotation on the *OA* section keeps as a constant or a convex line, and the rotation is only influenced by the constraints on the bolt head. When the relative displacement is large (10 mm), the rotation on the *OA* section show a concave line, and the moments show an increasing trend following a quick decreasing process (Fig. 8).

From Fig. 8 we can see how the negative moment reaches the maximum value near the joint *A*, and rapidly reduce to 0. In addition, the positive moments have the maximum value at the point *B* or near it: the maximum positive moment is larger than the negative one considered as absolute value.

From Fig. 9 is possible to note how the axial deformation on the endpoint *O* has a significant influence on the bolt deformation along the axial direction of the bolt: the axial displacement on the endpoint *C* for Case 1 is about 2.1 mm, and the one for Cases 2, 3 and 4 are 3.4 mm for a segments relative displacement of 10 mm. However, the constraints on the rotation and on the transversal displacement does not affect the axial displacement and the normal force along the bolt (Fig. 9 and Fig. 10). On Fig. 10, the normal force keeps as a constant on the *OB* section, and then tend to 0 on the endpoint *C*. It is obvious that the normal force when the endpoint is fixed in the axial direction (0.69 MN) is larger than the one (0.37 MN) when the bolt head is free to move in the axial direction.

Based on the analyses from Fig. 5 to Fig. 10, the maximum shear force is reached on the joint *A* and in the thread part (*BC* section), and the maximum moment near the joint *A* and the point *B*. Because the normal forces keep as a constant on the *OB* section, the critical points *A* and *B* are the high-risk locations of the bolt. From the results of the inclined bolt shear tests by He et al. (2021), the bolt produce a plastic hinge at the joint (Point *A*) and at the interface (Point *B*) between the thread and shank part of the bolt.

The constraints on the bolt head regarding the transversal displacement and the rotation, have a significant influence on the distribution of the shear force and the moment along the bolt on the *OA* section, but does not affect the axial displacement and the normal force. When a

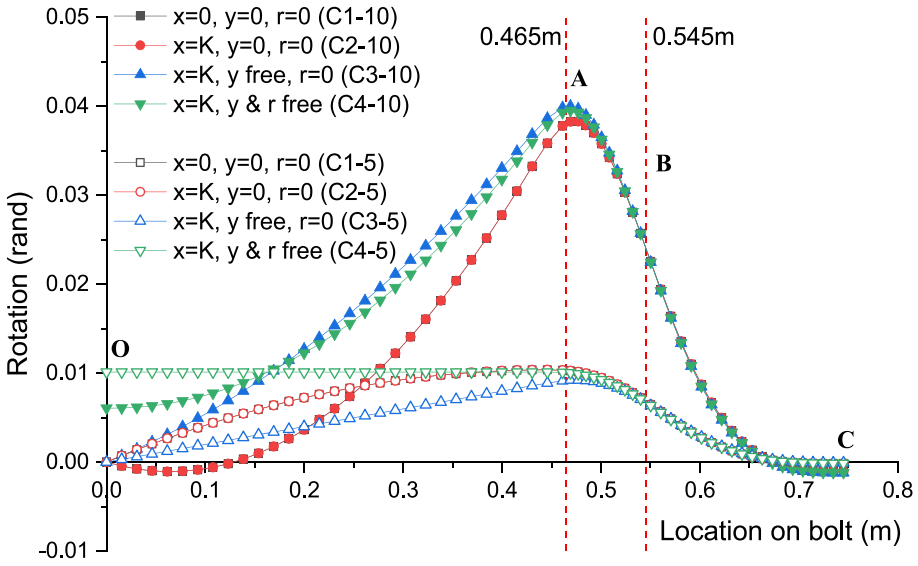

Fig. 7. Calculated rotation angles along the bolt.

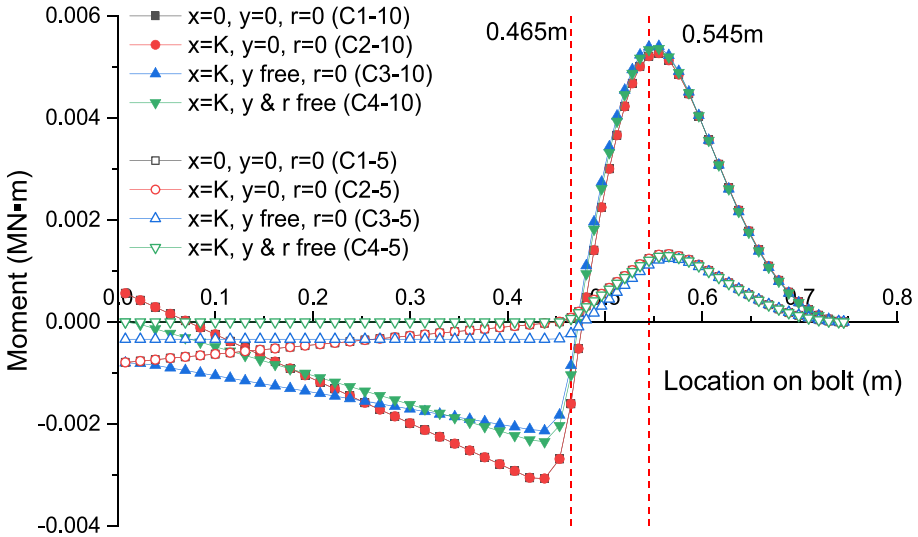

Fig. 8. Calculated moments along the bolt.

constraint prevents rotations and transversal displacements on the bolt head, the bolt has a larger value of the maximum shear force and moment. The axial displacement is mainly influenced by the axial constraints on the bolt head. An interesting aspect is that the contact between the bolt and the hole wall after a certain relative displacement of the segments on the joint not only leads to an increase of the value of the maximum shear force and moment in the bolt, but also affects the distribution of shear forces and moments along the bolt.

(2) The influence of the pre-tension and of the inclination angle on the developed bolt forces.

In order to control the shear deformation of the segmental lining on the circular joints, a pre-tension force is applied on the bolt head during the tunnel construction. Based on the developed analyses it became clear how the axial constraint at the bolt head has not any influence on the transversal displacements and rotations; an influence can be seen on the axial deformation and on the normal forces. When the bolt has a specific inclination angle with the joint, the relative displacements of the segments induce different axial and transversal deformations of the bolt and the induced forces in the bolt are also affected by this angle.

The calculated results are shown on Figs. 11 and 12 for different pre-tension forces on the bolt head (the pre-tension force varies from 0 to 100 MPa, keeping the inclination angle equal to 0°) and inclination angles of the bolt (the inclination angle varies from 0° to 50°, keeping the pre-tension force equal to 0), when the segments have a relative displacement of 10mm along the joint.

From Fig. 11 we can see how the pre-tension force in the bolt does not influence the shear force on the joint (it keeps as a constant), while leads to an increase of the normal force. Due to the fixed constraints on the endpoint *O* for Case 1, the normal force also keeps as a constant value. Finally, the increase of the pretension force leads to a slight increase of the applied force on the joint.

In Fig. 12 is possible to see how the inclination angle of the bolt has a significant effect on the shear and normal forces in the bolt on the joint. With the increase of the inclination angle the normal force has an obvious increase and the shear force a decrease. Under the comprehensive influence of both of them, the applied force on the joint shows an increase trend with the inclination angle. The inclination angle can therefore be optimized in order to synchronously reach the limit condition for both the shear force and the normal force of the bolt.

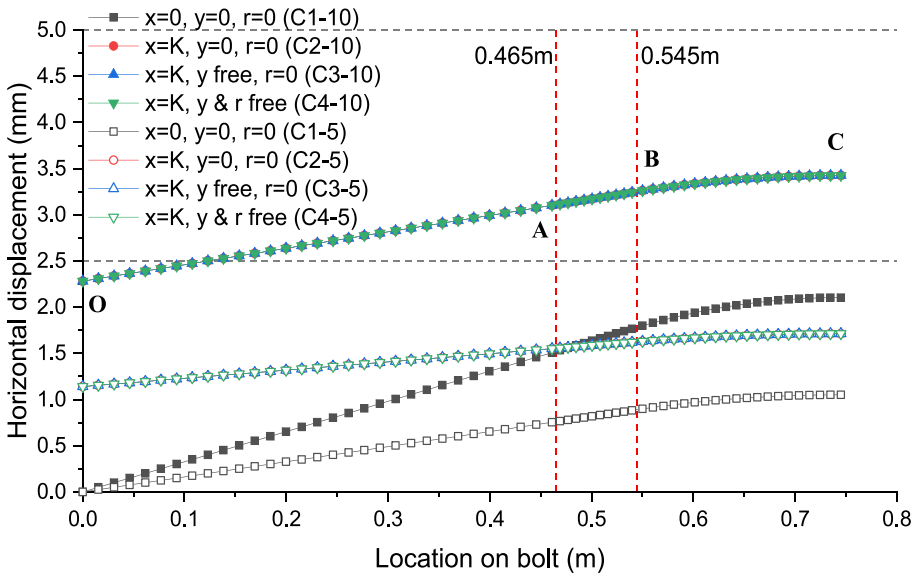

Fig. 9. Calculated axial displacements along the bolt.

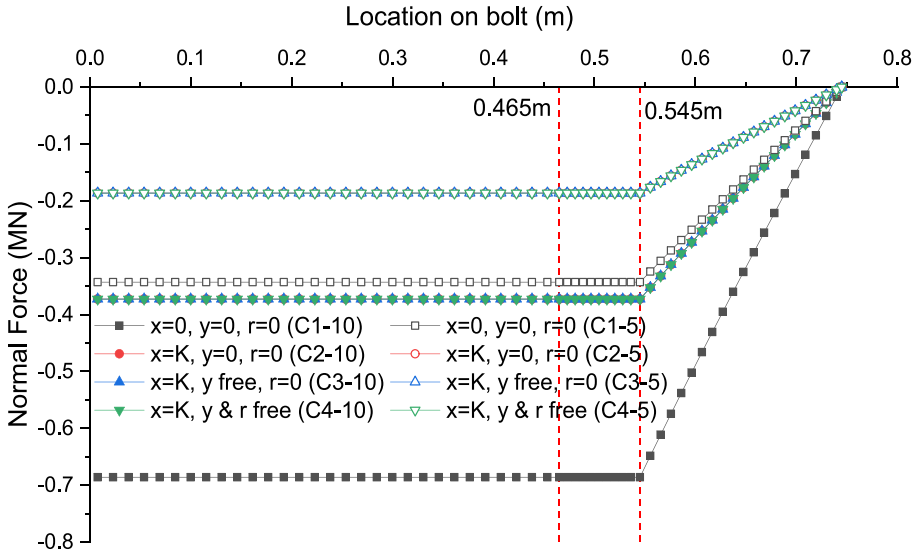

Fig. 10. Calculated axial forces along the bolt.

4. Main influential parameters on the joint shear stiffness

4.1. The influence of the gap distribution on the joint shear stiffness

On Sect.3, the influence of the constraints on the bolt head, the pretension force and the angle of inclination on the bolt deformation and the internal force distribution were discussed. Furthermore, the gap between the bolt and bolt hole is not uniform along the bolt axial direction based on Table.1; three key diameters determine the gap distributions: $d_{min,h,l}$, $d_{max,h,l}$ and $d_{max,h,r}$, which are called first diameter, second diameter and third diameter (d1st, d2nd, d3rd). Based on the real case No.3 of Table.1, the following parameters are adopted to analyse the deformation of an inclined bolt during relative shear displacements along the circumferential joint (Table 5).

Based on Eq.23, the shear stiffness of the circular joint K_{eq} can be obtained by the bolt deformation, considering each increasement of the relative displacement of the segments equal to 0.2 mm. The values of the calculated shear stiffnesses of the joint are shown in Fig. 13.

From Fig. 13, it is possible to see how the shear stiffness values are located in the range from the minimum value 34.96MN/m to the maximum one 67.80MN/m. When the gaps are equal to 0 mm (the diameters of bolt holes are 36 mm), the shear stiffness reaches the maximum value. When the gaps are larger than 0 mm, the shear stiffness starts from the minimum value where there is a small initial relative displacement, and then the shear stiffness increases and reaches the maximum value finally. Evaluating the effect of the diameters of the bolt hole, the second diameter ($d_{max,h,l}$) determines the starting point of the increase of the shear stiffness, and the third diameter ($d_{max,h,r}$) influences the slop of the increasing line. The increasing of the second diameter will lead to the elongation of the zone of minimum shear stiffness, and the increasing of the third diameter will lead to the decrease of the inclination of the slope of the shear stiffness trend with the relative displacement.

On the basis of Eq.23, the shear stiffness of the joint is influenced by the bolt shear and tensile stiffnesses and the angle of inclination of the bolt. For the studied case, the angle of inclination of the bolt is constant: it means that a straight bolt is considered. The tensile stiffness of the bolt $K_{eq,N}$ depends on the bolt tensile deformation and also on the compres-

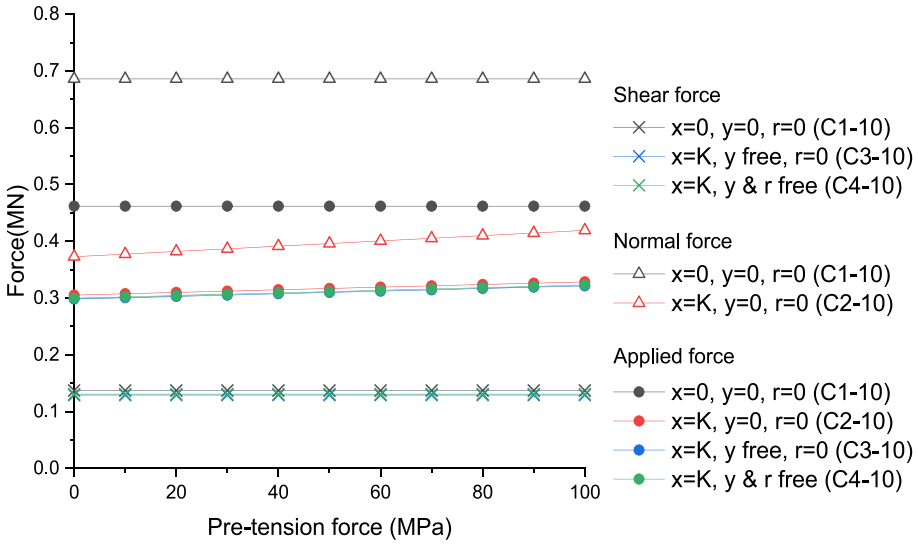

Fig. 11. The shear, normal and applied force on the joint as the pretension force varies. The shear force of the C2-10 case is equal to the C1-10 one and is not shown in the figure; the normal forces of the C3-10 and C4-10 cases are equal to the C2-10 one and is not shown in the figure).

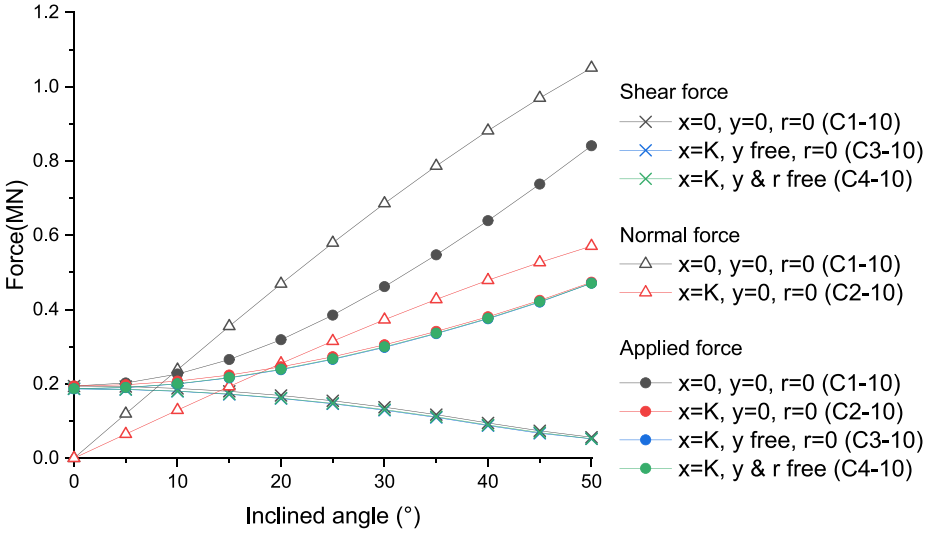

Fig. 12. The shear, normal and applied force on the joint as the inclination angle of the bolt varies. The shear force of the C2-10 case is equal to the C1-10 one and is not shown in the figure; the normal forces of the C3-10 and C4-10 cases are equal to the C2-10 one and is not shown in the figure).

Table 5
Key parameters adopted to calculate the inclined bolt shear deformation during relative shear displacements along the circumferential joint.

d_b(mm)	α(°)	Left segment			Right segment			d1st, d2nd, d3rd
		$d_{min,h,l}$(mm)	$d_{max,h,l}$(mm)	$l_{bolt,l}$(mm)	$d_{max,h,r}$(mm)	$l_{bolt,rs}$(mm)	l_{thread}(mm)	
M36	30	36	36	465	36	80	200	36,36,36
M36	30	42	42	465	42	80	200	42,42,42
M36	30	42	52	465	42	80	200	42,52,42
M36	30	42	52	465	52	80	200	42,52,52
M36	30	42	52	465	68	80	200	42,52,68
M36	30	52	52	465	52	80	200	52,52,52

sive deformation of the concrete surface below the steel plate at the bolt head (the detailed derivation of Eq.26 is shown on Appendix. A):

$$K_{eq,N} = \frac{1}{\frac{\coth(\rho \bullet l_{thread})}{E \bullet A_b \bullet \rho} + \frac{l_{shank}}{E \bullet A_b} + \frac{1}{K_{x,o}}} \tag{26}$$

where parameter ρ can be determined by Eq. A11 based on Eq.A6, $K_{x,o}$ is the compressive stiffness and can be obtained by Eq.16.

When the deformation of concrete surface below the steel plate is ignored, the last term on Eq.26 can be deleted.

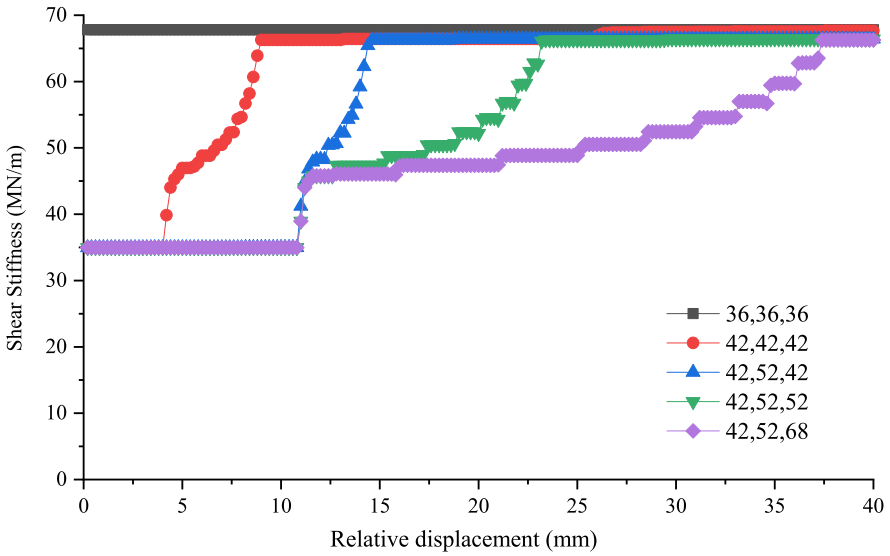

Fig. 13. The shear stiffness of the circular joint for different gap values varying the relative displacements between the segment rings (constraint case C1: x = 0, y = 0, r = 0).

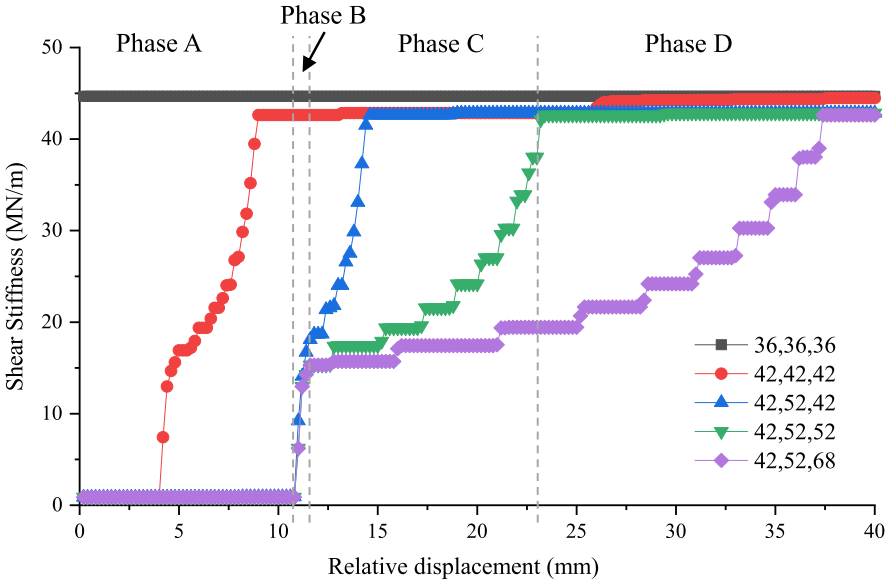

Fig. 14. The shear stiffness $K_{eq,Q}$ for different gap values varying the relative displacements between the segment rings (case of constraint type C1: x = 0, y = 0, r = 0).

4.2. The shear deformation and the shear stiffness of the straight bolt with zero angle of inclination

Focusing on the shear stiffness of the bolt $K_{eq,Q}$, this value is not a constant due the changeable of the constraint from the hole wall (Fig. 5 to Fig. 8); it can be calculated on the basis of Eq.24, and results are shown in Fig. 14.

Comparing Fig. 14 with Fig. 13, the trend of the shear stiffness is similar: it means that the nonlinear behaviour of the joint shear deformation is due to the bolt shear deformation in the bolt hole. From Fig. 14, when the diameter of the bolt hole is equal to the diameter of the bolt, the shear stiffness of the bolt reach the maximum value: it is also the limit maximum value for the other conditions when the gaps are larger than 0. The shear stiffness of the bolt can be divided into four phases based on the development of the relative displacement (Fig. 14, with reference to the case of hole diameters 42,52,52). When the diameter of the bolt hole is larger than the bolt, the shear stiffness of the bolt is initially low for relative displacements of the segments small (Fig. 14). At this phase, the bolt deforms under the constraint of the thread part and there are no constraints from the hole wall on the shank section (Fig. 15a): the deformation is obtained by the calculated results of the developed FEM model. With the increase of the relative displacement of the segments, the bolt contacts with the bolt hole near the joint on the left segment (Fig. 15b), and the shear stiffness starts to increase (Fig. 14). Furthermore, the bolt in the section *AB* starts to contact with the concrete on the bolt hole near the point *B* (Fig. 15c). From Fig. 14, the phase *B* is very short, and the shear stiffness has a quick increase. When all the bolt in the section *AB* contacts with the hole wall (Fig. 15d), the shear stiffness of the bolt reaches a value that is close to the maximum one. Therefore, the transversal displacement of the bolt near the joint on the left segment determines the contact between the bolt and the hole wall, and when the value of the transversal displacement is equal to the gap the starting point of the increase of the shear stiffness (Fig. 13 and Fig. 14) is reached. On the other hand, when the

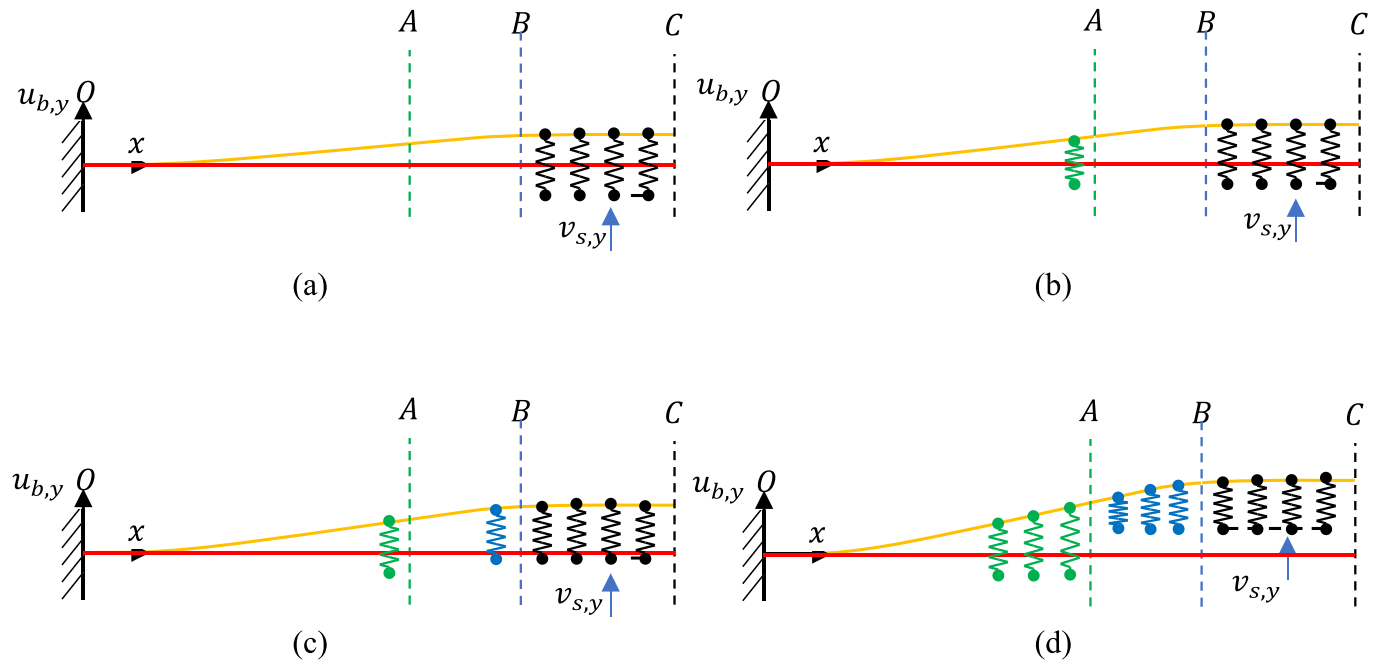

Fig. 15. The constraints on the bolt from the hole wall with the increase of the relative displacement of the segments on the circular joints (case of type of constraint C(1): x = 0, y = 0, r = 0). Key: (a) phase A: no constraints from the hole wall; (b) phase B: the bolt in the section *OA* starts to contact with the hole wall; (c) phase C: the bolt in the section *AB* starts to contact with the hole wall; (d) phase D: the whole length of the bolt in section *AB* contacts with the hole wall. ($u_{b,y}$ represents the bolt transversal deformation along the bolt on the local coordinate x-y, $v_{s,y}$ represents the y-component of the relative displacement of the right segment lining corresponding to the left one).

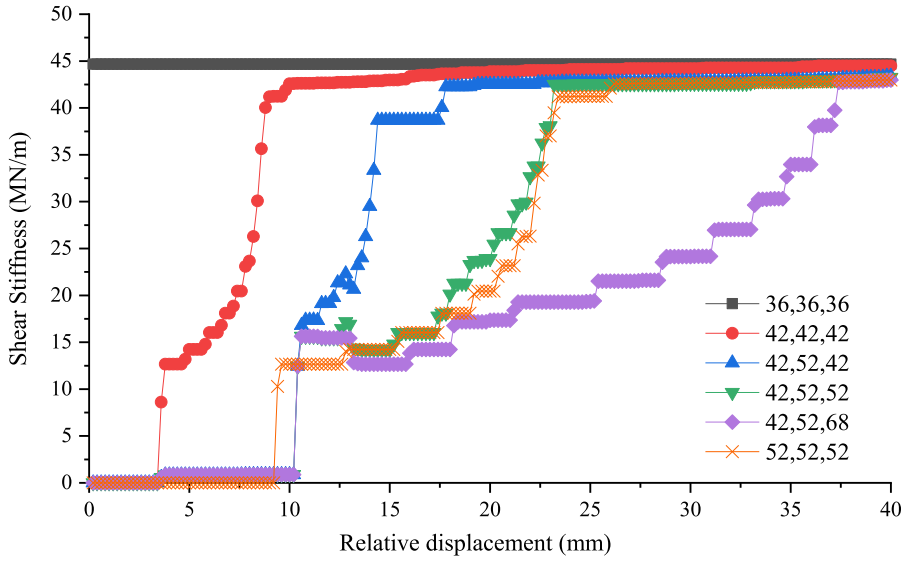

Fig. 16. The shear stiffness $K_{eq,Q}$ for different gap values varying the relative displacements between the segment rings(type of constraint C(3): x = K, y free, r = 0).

bolt contacts the bolt hole in the section *AB*, the point where the shear stiffness of the bolt is close to its maximum value is reached.

Due to the same constraints of the transversal displacements and of the rotations on the bolt head for the Case 1 and 2, the shear stiffness of the bolt also is the same as those two cases. In order to know the influence of the other constraints on the bolt head, the shear stiffness of the bolt for Case 3 and Case 4 are shown in Fig. 16 and Fig. 17.

From Fig. 14, Fig. 16 and Fig. 17, it is possible to see how the shear stiffnesses of the bolt have a similar trend for different constraint types on the bolt head. The maximum and the minimum values of the shear stiffnesses are resumed in Table.6: the constraint types on the bolt head have a very small effect on the maximum value of the shear stiffness. When the constraints of the transversal displacements on the bolt head is free, the minimum shear stiffness of the bolt is equal to 0, and has a slightly increasement at the starting range. The constraints on the bolt head affect the development of the shear stiffnesses with the relative displacements on the circular joint (Fig. 18).

The development of the shear stiffness of the bolt can be divided into three parts with an increase of the relative displacements between segments: part I, part II and part III of Fig. 18. In the part I, the shear stiffness of the bolt has the minimum value (close to 0). In the part II, the shear stiffness of the bolt increases from the minimum value to the maximum one, and the increase of the shear stiffness is nonlinear. In order to improve the practicality in the shear stiffness evaluation, the

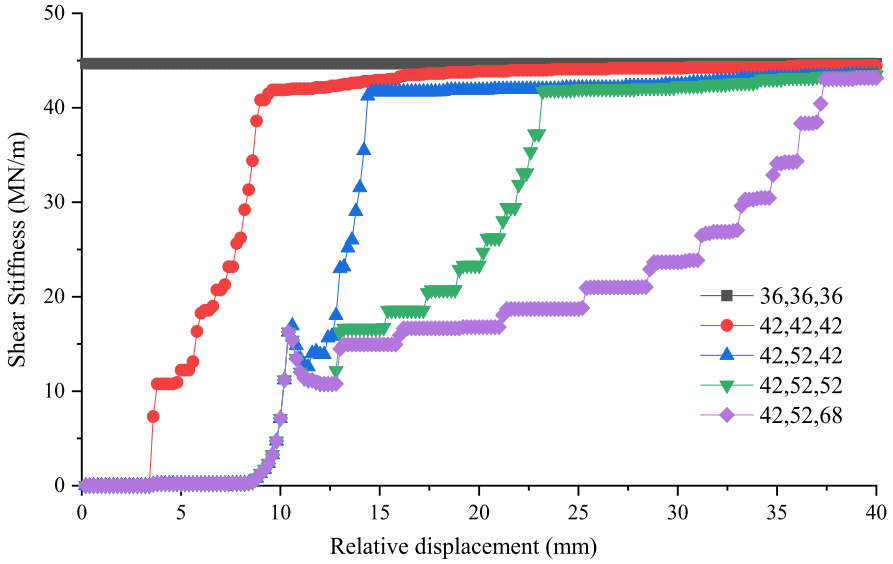

Fig. 17. The shear stiffness $K_{eq,Q}$ for different gap values varying the relative displacements between the segment rings C(4): x = K, y & r free).

Table 6
The comparison of the maximum and minimum shear stiffnesses of a straight bolt (zero angle of inclination) for different constraint types on the bolt head.

	Maximum shear stiffness (MN/m)	Minimum shear stiffness (MN/m)
C1: x = 0, y = 0, r = 0	44.6730	0.8840
C2: x = K, y = 0, r = 0	44.6730	0.8840
C3: x = K, y free, r = 0	44.6727	0
C4: x = K, y & r free	44.6727	0

shear stiffness in the part II can be considered as a linear line (Fig. 18). In the part III, the shear stiffness of the bolt is close to the maximum value, which is referred to a gap value of 0. By this approach, the shear stiffness of the bolt can be simplified by a multiple polyline (as the red dashed lines of Fig. 18). Therefore, the complex trend of the shear stiffness of the bolt varying the relative displacements between segments is simplified by determining three key parameters: the displacement at the starting point and at the final point and the maximum value of the stiffness.

4.3. The determination of key parameters of the simplified approach for the bolt shear simulation

Based on the analysis of the bolt deformation of the last section, the shear stiffness of bolt change remarkably when a constraint from the concrete hole wall appears. The three key parameters can be obtained by the following three models (Figs. 19, 20 and 21).

(1) The determination of the relative displacement at the starting point.

In the part I of Fig. 18 the bolt does not contact with the hole wall. At the end of part I, the bolt near the joint *A* begins to contact the hole wall. On the thread section *BC*, the bolt is restricted by the polyamide bolt sleeve, and the constraints on the point *B* can be simplified as a fixed constraint (Fig. 19). For the bolt head (point *O*), there are two types constraints based on whether bolt is stretched.

When the bolt is stretched and the concrete surface below the steel plate is compressed, the bolt head together with the washer will restrict the rotation and the transversal displacement of the bolt head. Therefore, the constraint on the bolt head (point *O*) can be simplified as a fixed

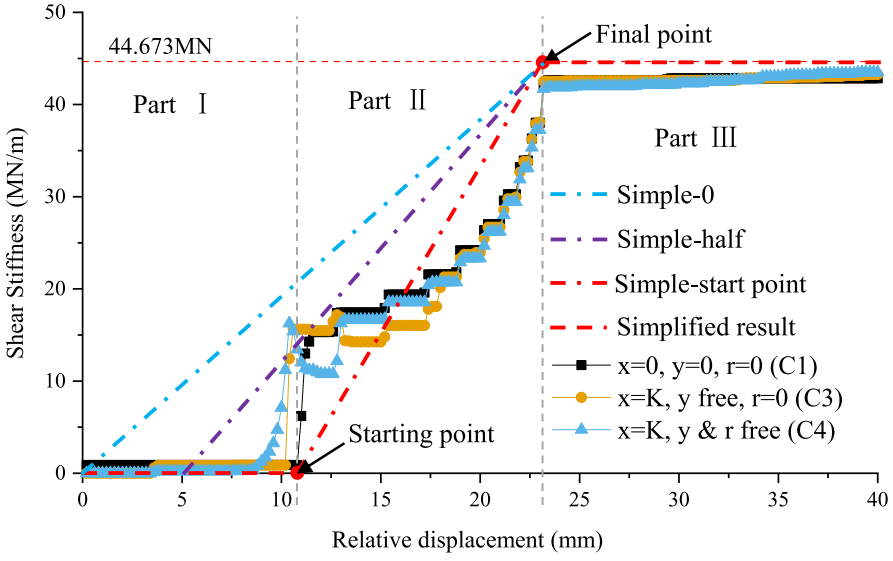

Fig. 18. The influence of the constraint type on the shear stiffness $K_{eq,Q}$ of the bolt and the simplified trends represented by the straight lines (the considered values of the bolt hole diameters are 42,52,52 mm as for Fig. 2).

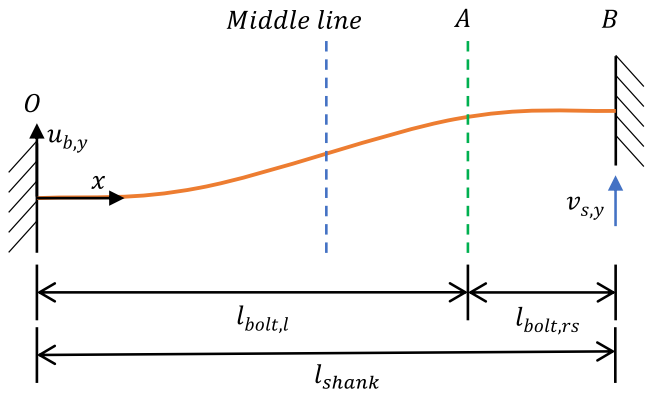

Fig. 19. The bolt deformation with the assumption of a fixed constraints on the bolt head.

one as shown in Fig. 19.

Based on the schematic diagram (Fig. 19), the transversal displacement along the bolt can be obtained by the following equation:

$$u_{b,y}(x) = \frac{F}{12 \bullet EI} \bullet x^2 \bullet (3 \bullet l_{shank} - 2 \bullet x) \tag{27}$$

where F is the applied force on the segment at the circular joint.

When the segments have a relative transversal displacement along the joint $v_{s,y}$, the ratio between the shear force and the relative displacement can be derived as:

$$\frac{F}{v_{s,y}} = \frac{12 \bullet EI}{l_{shank}^3} \tag{28}$$

Substituting Eq.28 into Eq.27, the relationship between the relative displacement $v_{s,y}$ of the segments in the point B and the transversal displacement $u_{b,y}(l_{bolt,l})$ of the joint A can be calculated by the following equation:

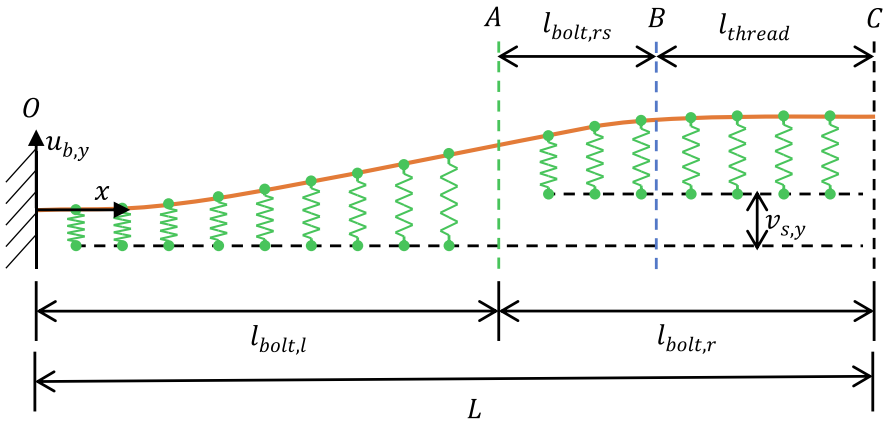

Fig. 20. The bolt deformation with fixed constraints on the bolt head.

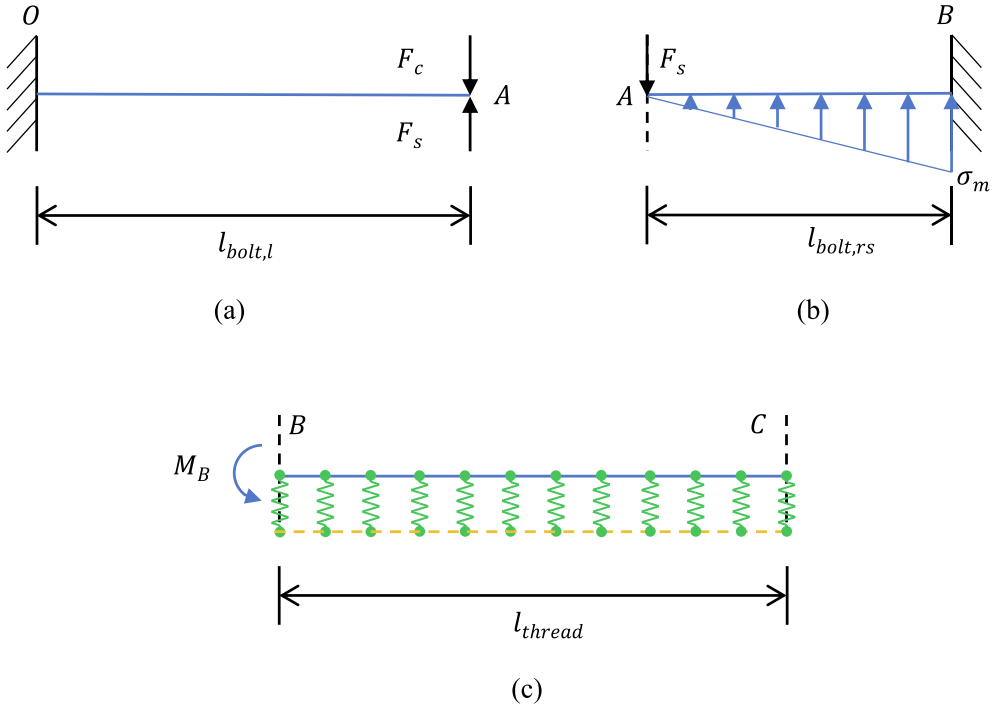

Fig. 21. The external actions and constraints on the three separated sections of the bolt. Key: (a) forces and constraints of the *OA* section; (b) *AB* section; (c) *BC* section.

$$u_{b,y}(l_{bolt,l}) = v_{s,y} \bullet \frac{l_{bolt,l}^2}{l_{shank}^3} \bullet (3 \bullet l_{shank} - 2 \bullet l_{bolt,l}) \tag{29}$$

When the vertical displacement $u_{b,y}(l_{bolt,l})$ on the joint A is equal to the half of the gap $(d_{max,h,l} - d_b)/2$, the shear stiffness of the bolt starts to increase quickly, and the relative displacement can be obtained:

$$L_{start} = v_{s,y} = \frac{d_{max,h,l} - d_b}{2} \bullet \frac{l_{shank}^3}{l_{bolt,l}^2 \bullet (3 \bullet l_{shank} - 2 \bullet l_{bolt,l})} \bullet \frac{1}{\cos(\alpha)} \tag{30}$$

where L_{start} represent the length of the part I and the value of the starting point on x-axis in Fig. 18.

On the other hand, there is no compressed force on the concrete surface below the steel plate and no constraints from the bolt head (point O) when the bolt is not stretched. The whole bolt has the same vertical displacement which is equal to the value on the point B, and the bolt reach to the concrete hole wall after a vertical displacement (a half of the gap). The relative vertical displacement of the segments can be derived:

$$L_{start} = v_{s,y} = \frac{d_{max,h,l} - d_b}{2} \bullet \frac{1}{\cos(\alpha)} \tag{31}$$

(2) The determination of the maximum shear stiffness

From Sect.4.1, the maximum shear stiffness can be evaluated when the gap is equal to 0 (Appendix B). In addition, the constraints at the bolt head have a small influence on the value of the maximum shear stiffness (Table.6). When the bolt is fixed at the bolt head, the constraints along the bolt are shown in Fig. 20.

The shear force on the joint can be obtained by the following equation.

$$T_A = v_{s,y} \bullet 2 \bullet E \bullet I \bullet \beta^3 \bullet \eta \tag{32}$$

where β is an intermediate parameter which depends on the concrete foundation compressive modulus and the elastic modulus of the bolt:

$$\beta = \sqrt[4]{\frac{E_s}{4 \bullet E \bullet I}} \tag{33}$$

where E_s is equal to $E_s = k_c \bullet d_b \bullet 1000$; k_c can be obtained by Eq.10; η is another parameter obtained by the length of bolt and the β parameter:

$$\eta = -\frac{a_1 + a_2 \bullet \cos(2\beta \bullet l_{bolt,l}) + a_3 \bullet \cos(2\beta \bullet l_{bolt,r}) + a_4 \bullet \sin(2\beta \bullet l_{bolt,l}) + a_5 \bullet \sin(2\beta \bullet l_{bolt,r}) + a_6 \bullet \sin[2\beta \bullet (l_{bolt,l} + l_{bolt,r})]}{a_7 + a_8 \bullet \cos[2\beta \bullet (l_{bolt,l} + l_{bolt,r})]} \tag{34}$$

where $a_1 - a_8$ parameters can be obtained as shown in Appendix.B.

Furthermore, the shear stiffness can then be obtained by Eq.24:

$$K_{eq,Q} = \frac{T_A}{v_{s,y}} = 2 \bullet E \bullet I \bullet \beta^3 \bullet |\eta| \tag{35}$$

(3) The determination of the final point of the relative displacement

In the part III of the trend of the shear stiffness (Fig. 18), the bolt on the AB section contacts with the concrete. The bolt in the OA section can be separated from the joint A, and the shear force from the bolt on the right side F_s and the compression reaction forces from the concrete hole wall F_c are applied to the bolt (Fig. 21a). For the point B, the moment reaches to the maximum value (Fig. 8), and the shear force tends to 0 (Fig. 6). Because the bolt in the joint A begins to contact with the concrete and the gap near the point B is equal to 0, the compressive reaction force of the concrete is assumed with a triangle distribution (the maximum value is σ_m) along the bolt axial direction (Fig. 21b). Furthermore, the external action on the BC section from the AB one in the point B is a moment (M_B). The bolt deformation on the BC section is influenced by the concrete hole wall presence (Fig. 21c).

With reference to Fig. 21b, the transversal displacement of the point A can be obtained by:

$$v_{per,1} = \frac{F_s \bullet l_{bolt,rs}^3}{3 \bullet EI} - \left(\sigma_m \bullet \frac{l_{bolt,rs}^4}{30 \bullet EI}\right) \tag{36}$$

where $v_{per,1}$ is a partial transversal displacement of bolt on point A based on the cantilever beam on Fig. 21b; in addition, another part of the transversal displacement is influenced by the rotation of bolt on point B, as Fig. 21c.

Since the shear force in point B tends to 0, the compressed reaction force can be derived by the equilibrium condition:

$$F_s = \frac{\sigma_m}{2} \bullet l_{bolt,rs} \tag{37}$$

The reaction moment in point B can then be obtained:

$$M_B = F_s \bullet l_{bolt,rs} - \frac{\sigma_m}{2} \bullet \frac{l_{bolt,rs}^2}{3} \tag{38}$$

Furthermore, the transversal displacement and the rotation of the point B in the BC section is obtained under the application of the moment M_B (Appendix C).

$$y_B = M_B \bullet \delta \tag{39}$$

$$\theta_B = M_B \bullet \varphi \tag{40}$$

where parameters δ and φ depend on the length of the BC section, the bolt characteristics, and the parameter β which can be calculated by Eq.33:

$$\delta = \frac{1}{2E \bullet I \bullet \beta^2} \bullet \frac{1 + h^2 - 2h \bullet \cos(2\beta \bullet l_{thread})}{1 - 4h + h^2 + 2h \bullet \cos(2\beta \bullet l_{thread})} \tag{41}$$

$$\varphi = -\frac{1}{E \bullet I \bullet \beta} \bullet \frac{-1 + h^2 + 2h \bullet \sin(2\beta \bullet l_{thread})}{1 - 4h + h^2 + 2h \bullet \cos(2\beta \bullet l_{thread})} \tag{42}$$

$$h = e^{2\beta l_{thread}} \tag{43}$$

Considering the influence of the bolt rotation on point B based on Fig. 21c, the total displacement of the joint A can be obtained by the following equation, which considers the rotation of bolt on point B:

$$v_{per} = \frac{F_s \bullet l_{bolt,rs}^3}{3 \bullet EI} - \left(\sigma_m \bullet \frac{l_{bolt,rs}^4}{30 \bullet EI}\right) + M_B \bullet \delta - M_B \bullet \varphi \bullet l_{bolt,rs} \tag{44}$$

Substituting Eq.37 and Eq.38 into Eq.44, it is possible to obtain:

$$v_{per} = F_s \bullet \left(\frac{4}{15 \bullet EI} \bullet l_{bolt,rs}^3 + \frac{2}{3} \bullet l_{bolt,rs} \bullet \delta - \frac{2}{3} \bullet l_{bolt,rs}^2 \bullet \varphi\right) \tag{45}$$

When the vertical displacement in the point A is equal to the half of the gap near the joint A on the right segment $(d_{max,h,r} - d_b)/2$, the shear force on the joint can be determined:

Table 7
Comparison between simplified method and proposed FEM model value of the maximum shear stiffness.

	FEM model	Simplified method	Percentage difference
Maximum shear stiffness (MN/m)	44.67	43.57	2.5 %

Table 8
Comparison of the starting point of relative displacement for different constraint types and bolt hole diameters using the proposed FEM model and the values that can be obtained by using simplified methods.

	Starting point of relative displacement by FEM model (mm)				Simplified methods	
	x = 0, y = 0, r = 0 (C1)	x = K, y = 0, r = 0 (C2)	x = K, y free, r = 0 (C3)	x = K, y & r free (C4)	Eq.30	Eq.31
42,42,42	4	4	3.4	3.4	3.68	3.46
42,52,42	10.8	10.8	10.2	8.8	9.81	9.24
42,52,52	10.8	10.8	10.2	8.8	9.81	9.24
42,52,68	10.8	10.8	10.2	8.8	9.81	9.24

Table 9
Comparison of the final point of relative displacement between the results of the FEM model and the simplified methods.

Diameters of the bolt hole	FEM model (mm)	Simplified methods (mm)	Percentage difference
42,42,42	9	8.24	8.9 %
42,52,42	14.6	14.37	1.6 %
42,52,52	23.4	21.96	6.2 %
42,52,68	37.4	34.11	8.8 %

$$F_s = \frac{15 \bullet EI}{\left(4 \bullet l_{bolt,rs}^3 + 10 \bullet EI \bullet \delta \bullet l_{bolt,rs} - 10 \bullet EI \bullet \varphi \bullet l_{bolt,rs}^2\right)} \bullet \frac{\left(d_{max,h,r} - d_b\right)}{2} \tag{46}$$

Based on the simplification of the shear stiffness trend as a linear line in part II of Fig. 18, the shear force at the final point can be obtained by the maximum shear force and the relative displacements of part II.

$$F_s = \frac{1}{2} \bullet K_{eq,Q} \bullet L_{partII} \tag{47}$$

Substituting Eq.46 into Eq.47, the length of the part II can be derived:

$$L_{partII} = \frac{2}{K_{eq,Q}} \bullet \frac{15 \bullet EI}{4 \bullet l_{bolt,rs}^3 + 10 \bullet EI \bullet \delta \bullet l_{bolt,rs} - 10 \bullet EI \bullet \varphi \bullet l_{bolt,rs}^2} \bullet \frac{d_{max,h,r} - d_b}{2} \tag{48}$$

where $K_{eq,Q}$ is obtained by Eq.35.

Furthermore, the location on x-axis of the final point on Fig. 18 can be obtained by the following equation:

$$L_{final} = L_{start} + L_{partII} \bullet \frac{1}{\cos(\alpha)} \tag{49}$$

(4) The comparison between the results of the developed FEM model and the simplified methods

On the basis of the parameters of Table 4 and Table 5, and the constraints types at the bolt head of Table 3, the results using the developed FEM model and the simplified method (maximum shear stiffness, relative displacements at the starting and final points) are calculated and listed in Table 7, Table 8 and Table 9. Since the constraints on the bolt head have a small impact on the maximum shear stiffness based of Table 6, the approximate value of the maximum shear stiffness (44.67MN/m) is adopted to compare the calculated results with the simplified method in Table 7. For the comparison of the relative displacements at the starting and final points, the influences of the constraints are considered.

How it is possible to see in Table 7, the percentage difference of the results of the simplified method compared with the proposed FEM model, is only 2.5 %. Furthermore, considering that the difference of the maximum shear stiffness for the different assumed constraints at the bolt head is small (Table 6), Eq.35 can be useful to quickly calculate the maximum shear stiffness of a bolt.

From Table 8 is possible to see how the constraint type n.4 has the minimum value of the starting point of relative displacement, and the type n.1 has the maximum one. Regarding the simplified methods, the results from Eq.30 are closer to the ones of the proposed FEM model for constraint types 1, 2 and 3, while Eq.31 is better for the constraint type n.4.

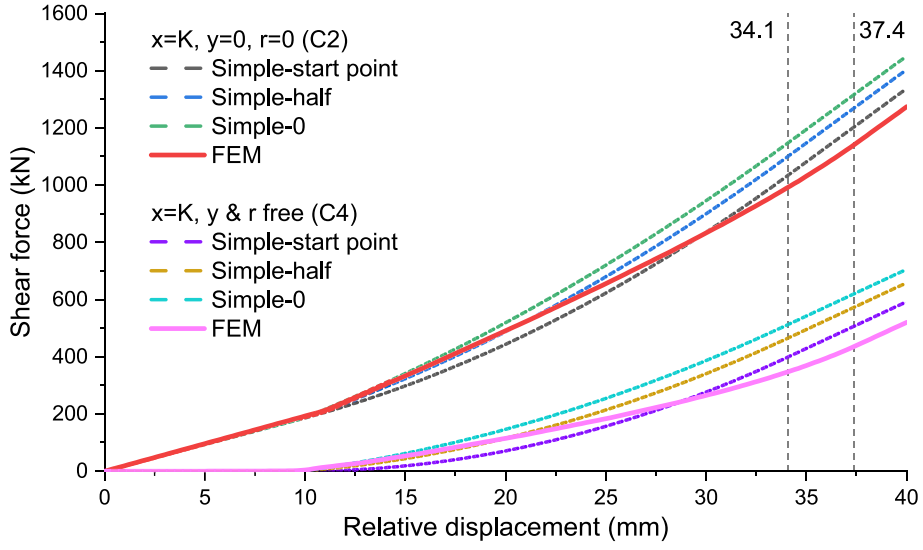

Fig. 22. Comparison of the shear force of the bolt, varying the relative displacement, calculated by the developed FEM model and the simplified methods. Key: simple-start point means that the first point on the horizontal axis is located on the starting point; simple-half means that the first point is located in the middle point of part I; simple-0 means that the first point of the trend line is located in the origin.

Table 10
Key parameters of the joint based on the studied case of He et al. (2021).

d_b(mm)	α(°)	Left segment			Right segment			Diameter of washer (mm)
		$d_{min,h,l}$(mm)	$d_{max,h,l}$(mm)	$l_{bolt,l}$(mm)	$d_{max,h,r}$(mm)	$l_{bolt,rs}$(mm)	l_{thread}(mm)	
M30	30	36	46	368	60	60	160	70

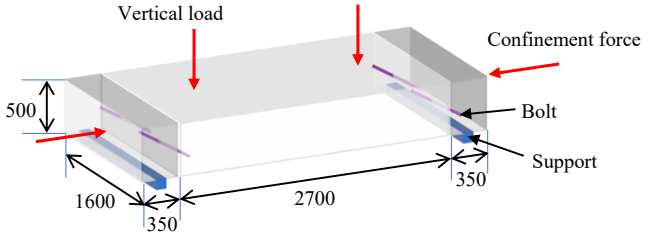

Fig. 23. Scheme of the tested structure and of the applied loads in the laboratory test by He et al. (2021). Lengths in mm.

The final point of relative displacements have a very small difference varying the type of constraint (Fig. 18); the comparison of the final point of relative displacement between the results of the FEM model and the simplified methods is shown in Table.9. The maximum percentage difference is about 8.9 %.

With reference to the three assumed trend lines of Fig. 18 in the part I and II of the graph, the shear forces are calculated by considering the presence of the tensile force and without the tensile force in the bolt (Fig. 22). When considering the tensile force presence, the bolt deformation is calculated on the basis of the constraints type n.2 (Table 3); the calculation is based on the constraints type n.4 when the tensile force in the bolt is disregarded.

From Fig. 22, we can see how the distribution of the shear stiffness in part II (Fig. 18) affects the development of the shear force varying the relative displacement on the circular joint. The FEM results have a good consistency with the ones of "simple-half" at the beginning zone of the graph (low relative displacements) which is very important in the analysis of the bolt deformation. However also the trend line of the shear stiffness which starts in the origin ("simple-0"; the blue line in Fig. 18) can be suggested to correctly evaluate the shear stiffness of the bolt in the circular joint.

5. Some examples of calculations of the shear stiffness of the circular joint

5.1. The validation of the shear simulation of the bolt

In order to validate the developed FEM model, the results from a laboratory test (He et al., (2021) are compared with the calculation results. The parameters of the case are listed in Table 10. The material parameters of the bolt and concrete are the same of Sect. 3. Since the inclined bolt is not perpendicular to the plane of the joint, the bolt head will compress the concrete when the angle between the relative displacement direction and the bolt axial direction is smaller than 90°, and the bolt is stretched along the axial direction. When the bolt is compressed, the constraints on the bolt head don't exist (non-tensile condition). On the basis of the test measurements (He et al., 2021) (Fig. 23), the comparison with the calculated results by the developed FEM model is shown in Fig. 24 for the tensile and the non-tensile conditions and two bolts in the joint. Since a friction shear force of about 300kN is present during the test, an initial shear force of 300kN is added into the FEM model.

For the tensile condition, the trend of the FEM results shows a good consistency with the test measurements. There are also some differences between the test results and the calculated ones. In Fig. 24, the shear force reduces suddenly at 526kN, and the main reason is the yielding of the materials. The joint shows a nonlinear behaviour during the test. As stated before, the developed FEM model only considers a structural nonlinear behaviour; no any sudden damage of the joint can be found in

Table 11
The shear stiffness of the bolt based on simplified methods.

Tensile stiffness (MN/m)	Maximum shear stiffness (MN/m)	Relative displacement at the starting point (mm)	Relative displacement at the final point (mm)
68.56	34.69	9.76	38.52

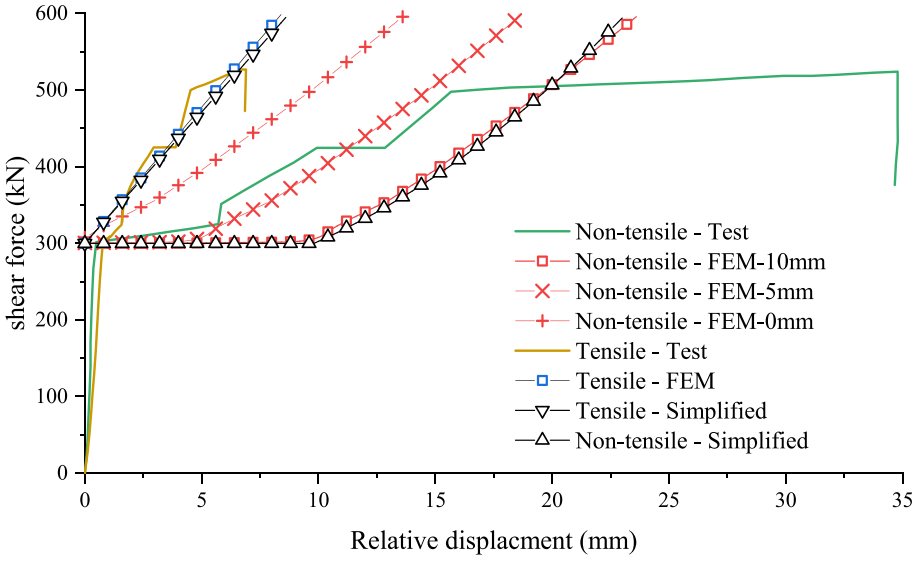

Fig. 24. Comparison between the test measurements of He et al., 2021 and the calculated values by the developed FEM model.

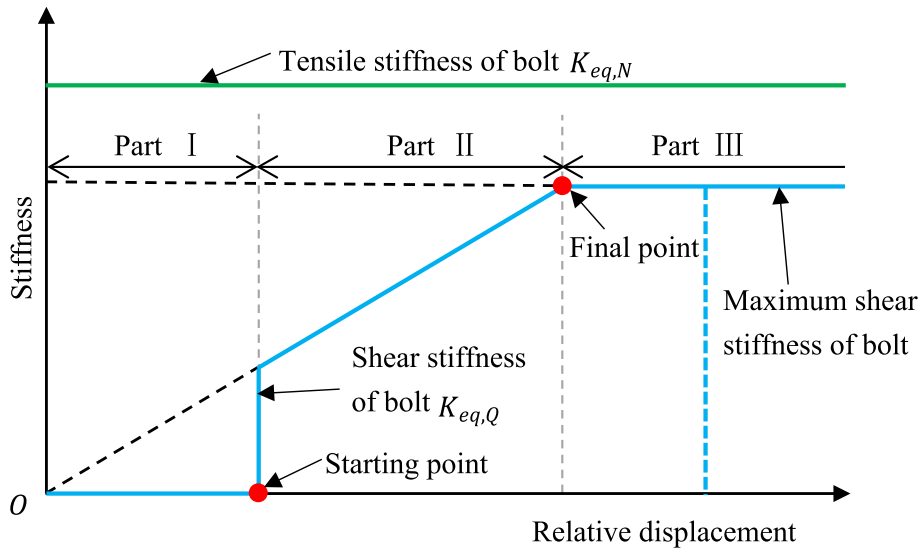

Fig. 25. The tensile stiffness and the shear stiffness of the bolt varying the relative displacements on the circular joint.

the figures due to the materials yielding and the same for the adopted simplified model. Although the shear force can continually increase with the segment relative displacement, all the curves are calculated until the shear force reaches 600kN.

For the non-tensile condition, the value of the initial gap is difficult to determine for the developed model when the lab test is simulated. Based on its design, there is about 10 mm gap between the bolt and bolt hole. However, during the lab test, it is very difficult to insert the bolt centering it in the hole. When the bolt is not in the center of the hole, the initial gap values can vary and influence the trend of the experimental curve, moving it of some different millimetres along the x axis. From Fig. 24 it is possible to see how the line referred to the FEM results with a gap of 5 mm has a good agreement with the test results. By the comparison between the test measurements and the calculated results using the developed FEM model, it is possible to see how this last one can effectively describe the joint shear deformation law of an inclined bolt.

Since the developed models are mainly focused on the nonlinear behaviour of the structure and on the elastic behaviour of the materials, they are able to analyse the joint shear deformation in the elastic phase. When the yielding of the materials is considered, some modifications need to be carried out in the models: they will be studied in a future research work.

On the other hand, the test results show that there are great differences between the tensile and non-tensile conditions. For the tensile condition, the bolt behaviour is mainly influenced by the tensile stiffness when the segments have a relative displacement (Eq.26 and Eq.23). For the non-tensile condition, there is no tensile deformation of the bolt, and the bolt behaviour is mainly affected by the its shear deformation in the bolt hole. This difference needs to be considered in the tunnel lining design.

Based on the simplified method of Sect.4.3, the tensile stiffness, the maximum shear stiffness, the starting point and the final point relative displacement can be obtained (Table 11). Furthermore, the shear forces with the relative displacements are calculated (Fig. 24). In Fig. 24 is possible to see how the shear force obtained from the simplified method has an effectiveness when the tensile condition of the bolt is adopted. When the bolt is not stretched, the simplified methods are close to the FEM model at the beginning section of the part II. The results show again that the trend line passing through the origin of the graph (Fig. 18) is adequate to correctly estimate the shear stiffness of the bolt.

5.2. The flow chart of the joint shear stiffness estimation using simplified methods

After the analysis developed in Sect.4, we can consider the tensile stiffness of the bolt as a constant value (the green line of Fig. 25); the shear stiffness of the bolt can be represented by the blue line of Fig. 25: three parts can be obtained varying the relative displacements. The shear stiffness of part I is equal to 0; the shear stiffness of the part II is represented by an inclined line which pass through the origin and reach the final point; the shear stiffness in part III keeps constant (the maximum shear stiffness of the bolt). In addition, the blue dotted line represents the suddenly decrease of the shear stiffness when the bolt or concrete reaches the material yielding condition. Since the yielding of the material is not considered in this paper, no limit values of the relative transversal displacements are suggested. The flow chart of the steps necessary to calculate the equivalent shear stiffness of a circular joint is represented in Fig. 26, using simplified methods.

In the Flow Chart of Fig. 26 there are two fundamental parameters: the concrete foundation compressive modulus and the concrete foundation shear modulus. In this paper, the evaluation method for the concrete foundation shear modulus is suggested in Appendix A. The concrete foundation compressive modulus was discussed in different scientific papers available in literature (Maekawa and Qureshi, 1997; Soroushian et al., 1987b; Vintzēleou and Tassios, 1986). However, since these two parameters depend on the material characteristic of the concrete and the bolt, laboratory tests can be performed in order to obtain their values with a satisfactory accuracy.

In addition, only an elastic behaviour of the concrete and of the bolt were considered in this paper. When the bolt yielding is considered, the shear stiffness of the bolt tends to 0.

5.3. The evaluation of the shear stiffness of the circular joint considering the presence of all the bolts around the ring

On the cross section of the circular joint, the inclined bolts point in different directions along the circle (Fig. 27); three points are taken as specific cases for analysing the bolt deformation when the adjacent segments have a relative transversal displacement along the joint. In Fig. 27, the green rectangle represents the earlier installed segmental lining ring (old one); the white one is the late installed ring (new one); the blue arrow means the advancement direction; the green arrows represent the vertical direction in the vertical section; the purple arrows is the horizontal direction in the horizontal section.

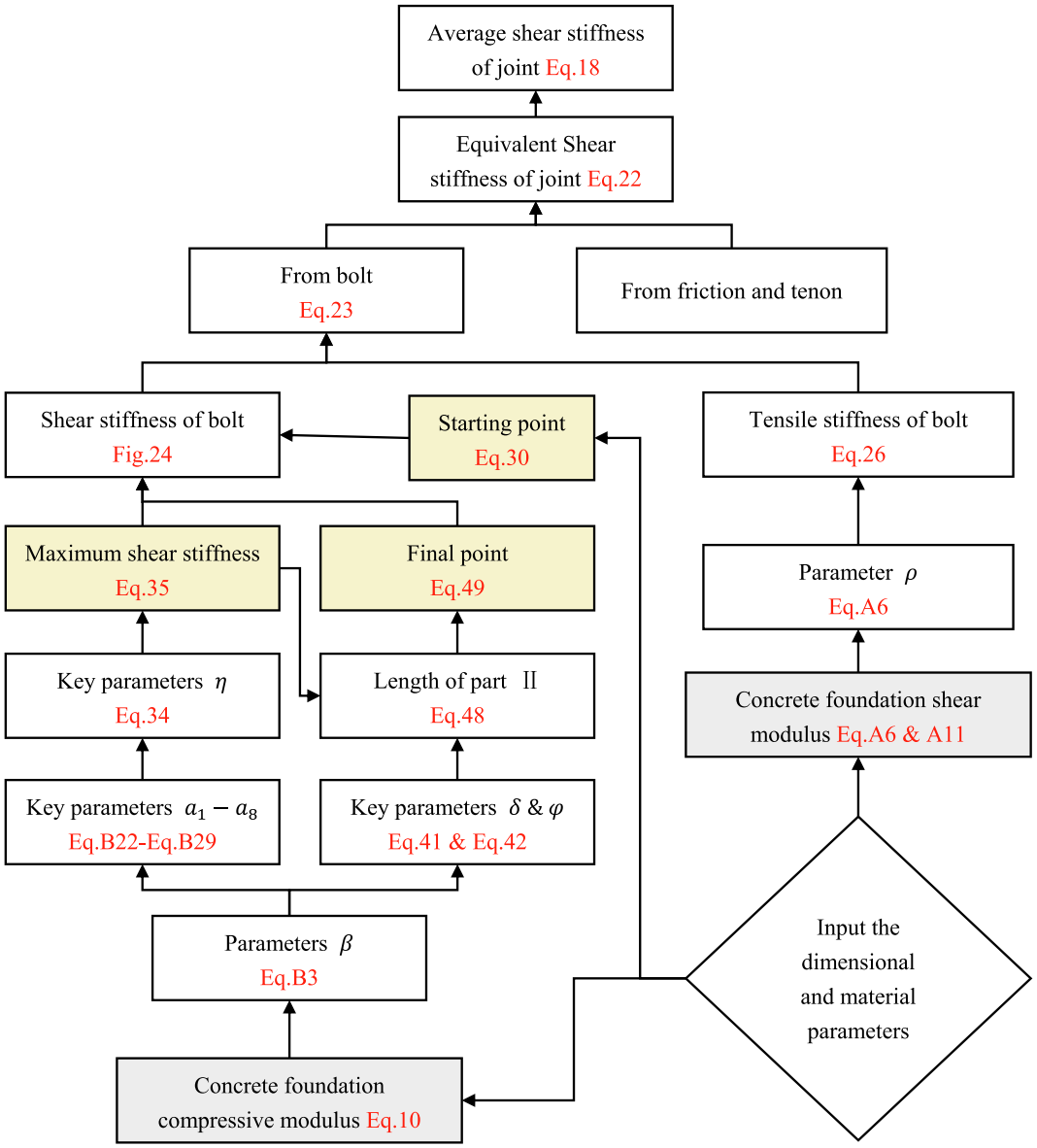

Fig. 26. The flow chart defined for the shear stiffness evaluation of the joint on the basis of simplified methods.

Therefore, the bolts have different deformation characteristics when the segments have a relative displacement. For example, the bolt is compressed in point 1, while the bolt is stretched in point 3, for the same upward displacement of the segments on the circular joint. On the basis of the analysis of Sect.5.1, the bolt in point 1 has the minimum shear stiffness and the bolt in point 3 has the maximum shear stiffness. Focusing on the bolt deformation in point 2, the displacement direction is perpendicular to the bolt axial direction, and the bolt is mainly affected by the shear deformation, where the deformation along the bolt axial direction can be ignored since there is no any displacement component along the axial direction. Therefore, the equivalent inclination angle of the bolt in point 2 can be considered as 0. The evaluation of the bolt equivalent inclination angle is important to calculate the joint shear stiffness.

For a general point 4, the tangent can be obtained on the joint cross section of Fig. 27 (the yellow line), and a radial line (red dotted line) represents the initial location. The schematic diagram of the bolt rotation from the initial line (red dotted line) to the real location (red line) with the tangent line is shown in Fig. 28, where R represents the length of the bolt.

The equivalent inclination angle γ between the bolt and the horizontal plane is:

$$\gamma = \arcsin(\sin\omega \bullet \cos\vartheta) \tag{50}$$

where ω is the inclination angle of the bolt on the plane which is along the radial direction of the lining ring; ϑ is the location of the calculated bolt ($\vartheta \in [0, \pi]$); γ is the equivalent inclination angle of the bolt ($\gamma \in [-\alpha, \alpha]$). When $\gamma > 0$, the bolt is compressed, and the axial force can be ignored; otherwise, the shear stiffness of the joint is influenced also by the bolt tensile deformation.

Therefore, the shear stiffness can be calculated for each bolt along the circular joint. Furthermore, the total shear stiffness of the cross section of the circular joint can be obtained by summing up the shear stiffness of each bolt.

Usually, the joints in the segmental lining include the circumferential joints and the longitudinal ones; the bolts in the two types of joints have similar characteristics. Therefore, when an individual bolt deformation in the bolt hole is considered, the developed model for the bolt (as Fig. 4) can be adopted for any inclined bolt: the direction of the relative movements of the adjacent segments need to be determined based on

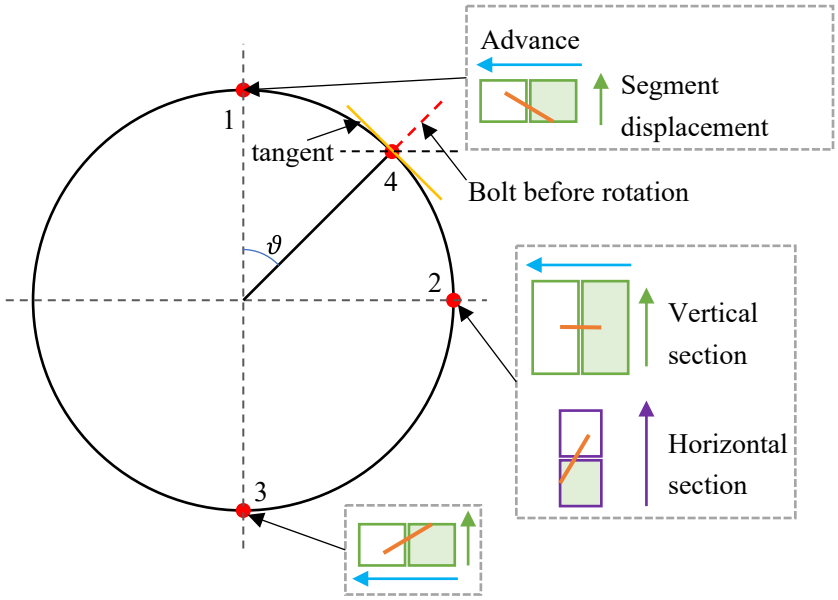

Fig. 27. The bolt deformation characteristic on the cross section of the circular joint. Legend: the green rectangle represents the earlier installed segmental lining ring (old one), and the white one is the late installed ring (new one); the blue arrows mean the advancement direction; the green arrows represent the vertical direction in the vertical section; the purple arrow is the horizontal direction in the horizontal section. (For interpretation of the references to colour in this figure legend, the reader is referred to the web version of this article.)

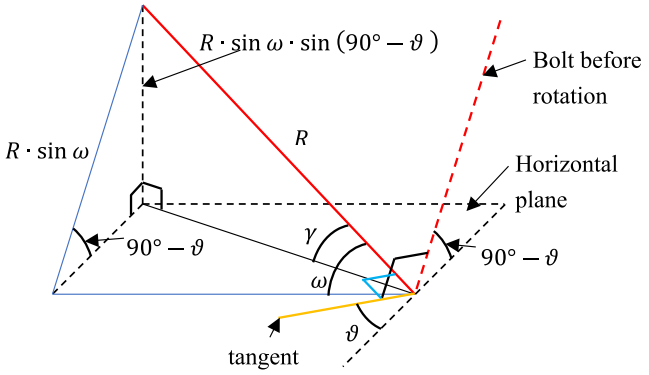

Fig. 28. 3D scheme for the calculation of the equivalent inclination angle γ on the circular joint.

Figs. 27 and 28. When the shear stiffness of joint is evaluated, the effect of all the bolts needs to be analysed based on its location in the joint. Due to a different distribution of the bolts in the two types of joints, the shear stiffness values have an obvious difference. In this paper only the role of the bolt for the joint shear stiffness was discussed; the contributions of tenons and of the friction forces between two adjacent segment faces were not considered. These two last effects need to be considered when the joint shear stiffness of a joint is determined.

6. Conclusions

During the deformation of the segmental lining along the longitudinal direction, the joint between the segmental rings has a weaker bending stiffness and shear stiffness than the ring. The evaluation of the shear stiffness for the joint is fundamental for the analysis of the lining

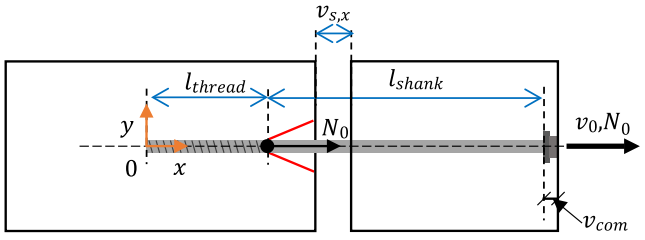

Fig. A2. The joint tensile deformation when there is a relative displacement of segments along the axial direction of the bolt.

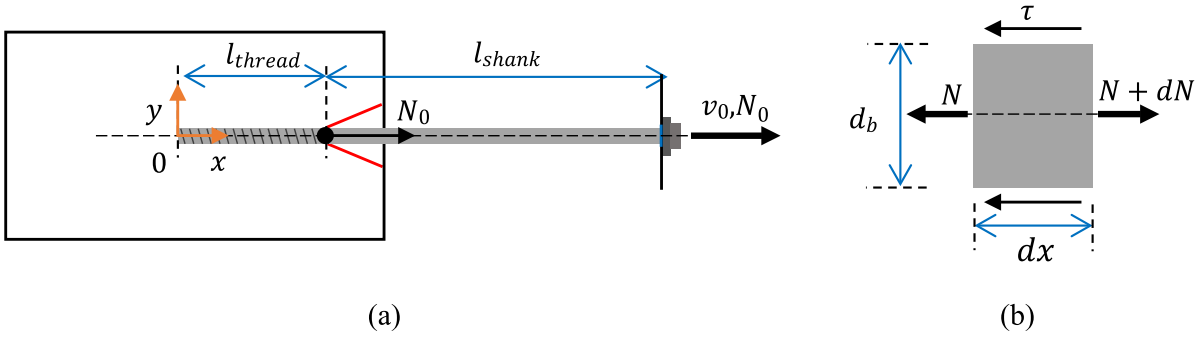

Fig. A1. The deformation of the bolt under a tensile force applied at the bolt head.

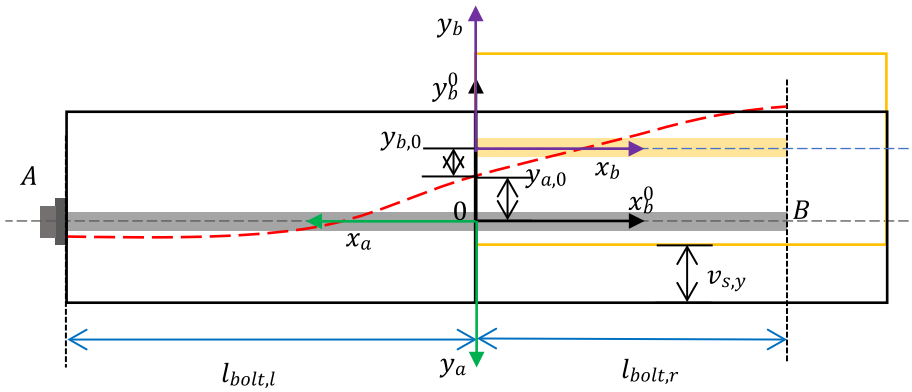

Fig. B1. The deformation of the bolt after a transversal relative displacement between the segments.

Table B1
The main imposed boundary conditions on the bolt (x and y constitute the coordinate system).

No.	Boundary conditions	No.	Boundary conditions
1	$y_a(x_a = 0) + y_b(x_b = 0) = -v_{s,y}$	5	$y_a(x_a = l_{bolt,l}) = 0$
2	$\theta_a(x_a = 0) = \theta_b(x_b = 0)$	6	$\theta_a(x_a = l_{bolt,l}) = 0$
3	$M_a(x_a = 0) = -M_b(x_b = 0)$	7	$M_b(x_b = l_{bolt,r}) = 0$
4	$T_a(x_a = 0) = T_b(x_b = 0)$	8	$T_b(x_b = l_{bolt,r}) = 0$

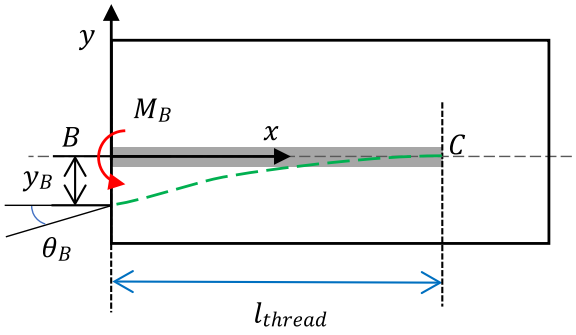

Fig. C1. The deformation of the bolt under a tensile force.

Table C1
The main boundary conditions of the bolt (x and y constitute the coordinate system).

No.	Boundary conditions ($x = 0$)	No.	Boundary conditions ($x = l_{thread}$)
1	$M(x = 0) = M_B$	3	$M(x = l_{thread}) = 0$
2	$T(x = 0) = 0$	4	$T(x = l_{thread}) = 0$

deformation and the damage risk. However, the shear stiffness and the shear deformation show a nonlinear behaviour. The main factors that result in the nonlinear behaviour are the friction, the bolt and the tenon presence. The nonlinear behaviour of the joint in the elastic phase is influenced by the bolt and is discussed in this paper.

Due to the existence of the gap between the bolt and the bolt hole and the uneven distribution of the gap, the range and the magnitude of the compressive forces on the bolt are changeable with the bolt deformation. A specific FEM model is proposed in this paper in order to calculate the bolt shear and tensile deformation with the relative displacement of adjacent segments; the relative equations are derived and illustrated. Based on the developed model, the transversal displacements, the shear forces, the rotations, the moments, the axial deformations and the tensile forces are evaluated considering four types of the constraints at the bolt head. The maximum shear forces are reached at the joint and the thread section, and the maximum moments are near the joint and the junction point between the thread and the shank of the bolt. These two locations (the joint and the junction point) have a high risk of yielding, which is also confirmed by the test results. Furthermore, the influences of the bolt pre-tension and the inclination angle are also analysed.

Based on the results of the shear force and the tensile forces along the bolt, the shear stiffness of the joint is obtained. It shows a nonlinear trend with the relative displacement of segments. Furthermore, the shear stiffness of the joint depends on the tensile stiffness and the shear stiffness of the bolt. For considering the nonlinear trend of the shear stiffness varying the relative displacement of segments, a simplified approach is developed and illustrated in the paper.

Finally, the shear deformation of the joint is validated by the comparison between some test results and the one from the developed FEM method: the results from the developed FEM method have a good consistency with the laboratory results of the tensile test; for the non-tensile test, the initial gap between the bolt and the bolt hole affects the test results, which have a good agreement with FEM model when some adjustments of the calculated results are made to consider some specific problems that can occur during the test. Furthermore, a flow chart for the calculation of the shear stiffness of the joint based on a simplified suggested method is proposed.

Based on the results obtained for the shear stiffness of the joint, a nonlinear law of the joint can be determined; the shear stiffness increases from an initial small value to a high value varying the relative transversal displacement. When the segmental lining deformation along the longitudinal direction is analysed, it is important to consider the influence of the small initial stiffness of a circular joint; in fact it may cause a significant increase of the joint dislocation and also of the surface subsidence.

CRediT authorship contribution statement

Xin Han: Conceptualization, Data curation, Formal analysis, Methodology, Software, Writing – original draft, Writing – review & editing. **Pierpaolo Oreste:** Conceptualization, Formal analysis, Methodology, Software, Supervision, Validation, Writing – original draft, Writing – review & editing. **Fei Ye:** Conceptualization, Funding acquisition, Investigation, Supervision, Validation, Visualization.

Declaration of competing interest

The authors declare that they have no known competing financial interests or personal relationships that could have appeared to influence the work reported in this paper.

Data availability

No data was used for the research described in the article.

Acknowledgment

This study was financially supported by the Fundamental Research Funds for the Central Universities, CHD (Grant No. 300102212702) and the National Natural Science Foundation of China (No. 52378389), and these support are gratefully acknowledged. The first author also would like to appreciate the scholarship from China Scholarship Council (Grant No. 202106560030) for his study in Politecnico di Torino.

Appendix A

In order to determine the concrete foundation shear modulus β_c on the thread part, the longitudinal tensile test can be used. The bolt deformation along the longitudinal direction is shown on Fig. A1a under the applied force N_0 at the bolt head.

Focusing on the bolt with a length of dx, the forces acting on the micro unit can be defined (Fig. A1b). Therefore, the following equation can be obtained:

$$dN = \pi \bullet d_b \bullet dx \bullet \tau \tag{A1}$$

where τ is the shear stress between the bolt and the bolt sleeve, and can be obtained by the concrete foundation shear modulus β_c and the relative displacement v.

$$\tau = \beta_c \bullet v \tag{A2}$$

Substituting the Eq.A2 into Eq.A1, the following differential equation can be derived:

$$\frac{dN}{dx} = \pi \bullet d_b \bullet \beta_c \bullet v \tag{A3}$$

Based on the constitutive equation of the bolt, the strain of the bolt is equal to the normal force over the elastic modulus and the area of the bolt cross section.

$$\frac{dv}{dx} = \frac{N}{E \bullet A_b} \tag{A4}$$

Therefore, the second order differential equation can be derived:

$$\frac{d^2v}{dx^2} - \frac{\beta_c \bullet \pi \bullet d_b}{E \bullet A_b} \bullet v = 0 \tag{A5}$$

where a parameter ρ is used to represent the constant coefficient.

$$\rho^2 = \frac{\beta_c \bullet \pi \bullet d_b}{E \bullet A_b} \tag{A6}$$

The general solution Eq.A7 of the differential equation Eq.A5 and boundary condition Eq.A8 can be derived.

$$v = H_1 \bullet e^{\rho \bullet x} + H_2 \bullet e^{-\rho \bullet x} \tag{A7}$$

$$\begin{cases} N = 0 & x = 0 \\ N = N_0 & x = l_{thread} \end{cases} \tag{A8}$$

Furthermore, the bolt deformation along the longitudinal direction can be obtained.

$$v = \frac{N_0}{E \bullet A_b \bullet \rho} \bullet \frac{e^{\rho \bullet x} + e^{-\rho \bullet x}}{e^{\rho \bullet l_{thread}} - e^{-\rho \bullet l_{thread}}} \tag{A9}$$

Therefore, the bolt deformation at the bolt head can be derived as:

$$v_0 = \frac{N_0}{E \bullet A_b \bullet \rho} \bullet \frac{e^{\rho \bullet l_{thread}} + e^{-\rho \bullet l_{thread}}}{e^{\rho \bullet l_{thread}} - e^{-\rho \bullet l_{thread}}} + \frac{N_0}{E \bullet A_b} \bullet l_{shank} \tag{A10}$$

The tensile stiffness of the composite structure is equal to the tensile force over the displacement of the bolt head:

$$K_{s,t} = \frac{N_0}{v_0} = \frac{E \bullet A_b}{\frac{\coth(\rho \bullet l_{thread})}{\rho} + l_{shank}} \tag{A11}$$

The concrete foundation shear modulus β_c can be derived by Eq.A6.

Based on the bolt deformation under the application of the tensile force, the bolt tensile deformation can be derived when there is a relative displacement of segments (Fig. A2). The relative displacement of segments can be calculated by the following equation:

$$v_{s,x} = v_0 + v_{com} \tag{A12}$$

where v_0 is the deformation of the bolt head and can be obtained based on Eq.A10; v_{com} is compressed deformation of the concrete surface blow the steel plate under the application of the bolt head, and is equal to the ratio between the compresses force and the compressed stiffness of the concrete $K_{x,o}$; $K_{x,o}$ can be calculated by Eq.16.

$$v_{com} = \frac{N_0}{K_{x,o}} \tag{A13}$$

Therefore, the relative normal displacement of the segments can be derived from the following equation:

$$v_{s,x} = \frac{N_0}{E \bullet A_b \bullet \rho} \bullet \frac{e^{\rho \bullet l_{thread}} + e^{-\rho \bullet l_{thread}}}{e^{\rho \bullet l_{thread}} - e^{-\rho \bullet l_{thread}}} + \frac{N_0}{E \bullet A_b} \bullet l_{shank} + \frac{N_0}{K_{x,o}} \tag{A14}$$

While, the tensile stiffness of the joint can be obtained:

$$K_{eq,N} = \frac{N_0}{v_{s,x}} = \frac{1}{\frac{\coth(\rho \bullet l_{thread})}{E \bullet A_b \bullet \rho} + \frac{l_{shank}}{E \bullet A_b} + \frac{1}{K_{x,o}}} \tag{A15}$$

Appendix B

When the gap between the bolt and the bolt hole is equal to 0, the compressed normal forces are applied on the bolt along its whole length. The bolt deformation with the relative transversal displacement of the segments can be considered as an elastic beam on the Winkler elastic foundation (Fig. B1).

Based on the theory of the Euler-Bernoulli beam on the Winkler elastic foundation, the differential equation of the beam for the coordinate system can be written by the following equation when the constraint on the bolt is due to compressive forces from the concrete hole wall.

$$E \bullet I \bullet \frac{d^4 y}{dx^4} + E_s \bullet y = 0 \tag{B1}$$

where E_s is compressive stiffness of the concrete hole wall.

The general solution of the Eq.B1 is as follows:

$$y = e^{\beta x} \bullet (B_1 \bullet \cos\beta x + B_2 \bullet \sin\beta x) + e^{-\beta x} \bullet (B_3 \bullet \cos\beta x + B_4 \bullet \sin\beta x) \tag{B2}$$

where β is a parameter that can be calculated by the Eq.B3; B_1, B_2, B_3 and B_4 are parameters that can be obtained by imposing the boundary conditions.

$$\beta = \sqrt[4]{\frac{E_s}{4 \bullet E \bullet I}} \tag{B3}$$

where E_s is equal to $E_s = k_c \bullet d_b \bullet 1000$.

Therefore, the first derivative, the second derivative and the third derivative can be obtained based on the general solution.

$$y' = \beta \bullet e^{\beta x} \bullet [B_1 \bullet (\cos\beta x - \sin\beta x) + B_2 \bullet (\sin\beta x + \cos\beta x)] + \beta \bullet e^{-\beta x} \bullet [B_3 \bullet (-\cos\beta x - \sin\beta x) + B_4 \bullet (-\sin\beta x + \cos\beta x)] \tag{B4}$$

$$y'' = 2 \bullet \beta^2 \bullet e^{\beta x} \bullet (-B_1 \bullet \sin\beta x + B_2 \bullet \cos\beta x) + 2 \bullet \beta^2 \bullet e^{-\beta x} \bullet (B_3 \bullet \sin\beta x - B_4 \bullet \cos\beta x) \tag{B5}$$

$$y''' = 2 \bullet \beta^3 \bullet e^{\beta x} \bullet [B_1 \bullet (-\sin\beta x - \cos\beta x) + B_2 \bullet (\cos\beta x - \sin\beta x)] + 2 \bullet \beta^3 \bullet e^{-\beta x} \bullet [B_3 \bullet (-\sin\beta x + \cos\beta x) + B_4 \bullet (\cos\beta x + \sin\beta x)] \tag{B6}$$

Furthermore, the moment and the shear force of the bolt can be obtained by the derivative equation.

$$\begin{cases} \theta(x) = y' \\ M(x) = E \bullet I \bullet y'' \\ T(x) = E \bullet I \bullet y''' \end{cases} \tag{B7}$$

Based on the boundary conditions of Table.B1, the parameters B_{1b}, B_{2b}, B_{3b} and B_{4b} can be derived:

$$B_{1b} = v_{s,y} \bullet \frac{\left(-1-m-2 \bullet m \bullet n - m^2 \bullet n\right) - m \bullet n \bullet \cos\left(2\beta \bullet l_{bolt,l}\right) - m \bullet n \bullet \cos\left(2\beta \bullet l_{bolt,r}\right) + m \bullet (1-n) \bullet \sin\left(2\beta \bullet l_{bolt,l}\right) + (1+m) \bullet m \bullet n \bullet \sin\left(2\beta \bullet l_{bolt,r}\right) - m \bullet n \bullet \cos\left[2\beta \bullet \left(l_{bolt,l} + l_{bolt,r}\right)\right]}{2 + 8 \bullet m \bullet n + 2 \bullet m^2 \bullet n^2 + 4 \bullet m \bullet n \bullet \cos\left[2\beta \bullet \left(l_{bolt,l} + l_{bolt,r}\right)\right]} \tag{B8}$$

$$B_{2b} = -v_{s,y} \bullet m \bullet \frac{(-1-m\bullet n)+(-1+n)\bullet\cos(2\beta\bullet l_{bolt,l})+n\bullet(1+m)\bullet\cos(2\beta\bullet l_{bolt,r})-n\bullet\sin(2\beta\bullet l_{bolt,l})+n\bullet\sin(2\beta\bullet l_{bolt,r})+n\bullet\sin[2\beta\bullet(l_{bolt,l}+l_{bolt,r})]}{2+8\bullet m\bullet n+2\bullet m^2\bullet n^2+4\bullet m\bullet n\bullet\cos[2\beta\bullet(l_{bolt,l}+l_{bolt,r})]} \tag{B9}$$

$$B_{3b} = -v_{s,y}\bullet n\bullet \frac{(1+2\bullet m+m\bullet n+m^2\bullet n)+m\bullet\cos(2\beta\bullet l_{bolt,l})+m\bullet\cos(2\beta\bullet l_{bolt,r})+m\bullet(-1+n)\bullet\sin(2\beta\bullet l_{bolt,l})+(1+m)\bullet\sin(2\beta\bullet l_{bolt,r})+m\bullet\cos[2\beta\bullet(l_{bolt,l}+l_{bolt,r})]}{2+8\bullet m\bullet n+2\bullet m^2\bullet n^2+4\bullet m\bullet n\bullet\cos[2\beta\bullet(l_{bolt,l}+l_{bolt,r})]} \tag{B10}$$

$$B_{4b} = v_{s,y}\bullet n \bullet \frac{(-1-m\bullet n)-m\bullet(-1+n)\bullet\cos(2\beta\bullet l_{bolt,l})+(1+m)\bullet\cos(2\beta\bullet l_{bolt,r})+m\bullet\sin(2\beta\bullet l_{bolt,l})-m\bullet\sin(2\beta\bullet l_{bolt,r})-m\bullet\sin[2\beta\bullet(l_{bolt,l}+l_{bolt,r})]}{2+8\bullet m\bullet n+2\bullet m^2\bullet n^2+4\bullet m\bullet n\bullet\cos[2\beta\bullet(l_{bolt,l}+l_{bolt,r})]} \tag{B11}$$

and then, also:

$$B_{1a} = (-B_{3b} - v_{s,y}/2) \tag{B12}$$

$$B_{2a} = B_{4b} \tag{B13}$$

$$B_{3a} = (-B_{1b} - v_{s,y}/2) \tag{B14}$$

$$B_{4a} = B_{2b} \tag{B15}$$

where m and n can be calculated by the β parameter and the lengths $l_{bolt,l}$ and $l_{bolt,r}$.

$$m = e^{2\beta l_{bolt,l}} \tag{B16}$$

$$n = e^{2\beta l_{bolt,r}} \tag{B17}$$

Furthermore, the shear force of the bolt at the joint can be obtained based on Eq.B7:

$$T(0) = E\bullet I\bullet y_b^{'''}(x_b = 0) \tag{B18}$$

Therefore, the shear force $T(0)$ can be calculated:

$$T(0) = 2\bullet E\bullet I\bullet\beta^3\bullet(-B_{1b}+B_{2b}+B_{3b}+B_{4b}) \tag{B19}$$

$$T(0) = 2\bullet E\bullet I\bullet\beta^3\bullet v_{s,y}\bullet\eta \tag{B20}$$

where η can be obtained by the following equations based on the parameters m and n:

$$\eta = -\frac{a_1+a_2\bullet\cos(2\beta\bullet l_{bolt,l})+a_3\bullet\cos(2\beta\bullet l_{bolt,r})+a_4\bullet\sin(2\beta\bullet l_{bolt,l})+a_5\bullet\sin(2\beta\bullet l_{bolt,r})+a_6\bullet\sin[2\beta\bullet(l_{bolt,l}+l_{bolt,r})]}{a_7+a_8\bullet\cos[2\beta\bullet(l_{bolt,l}+l_{bolt,r})]} \tag{B21}$$

$$a_1 = (1+m\bullet n)\bullet(-1-2m+2n+m\bullet n) \tag{B22}$$

$$a_2 = m\bullet(-1+n^2) \tag{B23}$$

$$a_3 = n\bullet(-1+m^2) \tag{B24}$$

$$a_4 = m\bullet(1-4n+n^2) \tag{B25}$$

$$a_5 = n\bullet(1+4m+m^2) \tag{B26}$$

$$a_6 = 2m\bullet n \tag{B27}$$

$$a_7 = 2+8m\bullet n+2m^2\bullet n^2 \tag{B28}$$

$$a_8 = 4m\bullet n \tag{B29}$$

Appendix C

Focusing on the bolt deformation on the thread section *BC* (Fig. C1), the bolt rotation and the displacement on the point *B* can be obtained under

the application of the moment M_B, based on the same equations of the Appendix.B (Eq.B1-B6). The constraints in the point B and C are listed in Table. C1.

Based on the boundary conditions of Table.C1, the parameters B_1, B_2, B_3 and B_4 can be derived:

$$B_1 = -\frac{M_B}{2E \bullet I \bullet \beta^2} \bullet \frac{-1 + h \bullet \cos(2\beta \bullet l_{thread}) + h \bullet \sin(2\beta \bullet l_{thread})}{1 - 4h + h^2 + 2h \bullet \cos(2\beta \bullet l_{thread})} \tag{C1}$$

$$B_2 = \frac{M_B}{2E \bullet I \bullet \beta^2} \bullet \frac{(1 - 2h) + h \bullet \cos(2\beta \bullet l_{thread}) - h \bullet \sin(2\beta \bullet l_{thread})}{1 - 4h + h^2 + 2h \bullet \cos(2\beta \bullet l_{thread})} \tag{C2}$$

$$B_3 = \frac{M_B}{2E \bullet I \bullet \beta^2} \bullet \frac{h^2 - h \bullet \cos(2\beta \bullet l_{thread}) + h \bullet \sin(2\beta \bullet l_{thread})}{1 - 4h + h^2 + 2h \bullet \cos(2\beta \bullet l_{thread})} \tag{C3}$$

$$B_4 = -\frac{M_B}{2E \bullet I \bullet \beta^2} \bullet \frac{\left(-2h + h^2\right) + h \bullet \cos(2\beta \bullet l_{thread}) + h \bullet \sin(2\beta \bullet l_{thread})}{1 - 4h + h^2 + 2h \bullet \cos(2\beta \bullet l_{thread})} \tag{C4}$$

where h can be calculated by the parameter β and the length l_{thread}.

$$h = e^{2\beta \bullet l_{thread}} \tag{C5}$$

Furthermore, the displacement on the point B can be obtained based on Eq.B7:

$$y_B = y(x = 0) \tag{C6}$$

Therefore, the displacement of the point B can be determined:

$$y_B = B_1 + B_3 \tag{C7}$$

$$y_B = \frac{M_B}{2E \bullet I \bullet \beta^2} \bullet \frac{1 + h^2 - 2h \bullet \cos(2\beta \bullet l_{thread})}{1 - 4h + h^2 + 2h \bullet \cos(2\beta \bullet l_{thread})} \tag{C8}$$

The rotation on the point B can be obtained as follows:

$$\theta_B = y'(x = 0) \tag{C9}$$

$$\theta_B = \beta \bullet (B_1 + B_2 - B_3 + B_4) \tag{C10}$$

$$\theta_B = -\frac{M_B}{E \bullet I \bullet \beta} \bullet \frac{-1 + h^2 + 2h \bullet \sin(2\beta \bullet l_{thread})}{1 - 4h + h^2 + 2h \bullet \cos(2\beta \bullet l_{thread})} \tag{C11}$$

References

Chaipanna, P., Jongpradist, P., 2019. 3D response analysis of a shield tunnel segmental lining during construction and a parametric study using the ground-spring model. Tunn. Undergr. Space Technol. 90, 369–382.

Chen, J.S., Mo, H.H., 2009. Numerical study on crack problems in segments of shield tunnel using finite element method. Tunn. Undergr. Space Technol. 24, 91–102.

Chen, Y., Wen, G., Hu, J., 2020. Analysis of Deformation Characteristics of Fully Grouted Rock Bolts Under Pull-and-Shear Loading. Rock Mech. Rock Eng. 53, 2981–2993.

Cheng, H.Z., Chen, R.P., Wu, H.N., Meng, F.Y., Yi, Y.L., 2021. General solutions for the longitudinal deformation of shield tunnels with multiple discontinuities in strata. Tunn. Undergr. Space Technol. 107.

Cowper, G.R., 1966. The Shear Coefficient in Timoshenko's Beam Theory. J. Appl. Mech. 6.

Ding, W., Chen, X., Jin, Y., Qiao, Y., 2021. Flexural behavior of segmental joint containing double rows of bolts: Experiment and simulation. Tunn. Undergr. Space Technol. 112.

Feng, K., He, C., Qiu, Y., Zhang, L., Wang, W., Xie, H., Zhang, Y., Cao, S., 2018. Full-scale tests on bending behavior of segmental joints for large underwater shield tunnels. Tunn. Undergr. Space Technol. 75, 100–116.

Feng, H., Ye, F., Jiang, Y., Wang, J., Wen, X., Fang, Q., 2022. Effect of rolling angle on segment cracking and damage of shield tunnel - field investigation and modelling. Eng. Fail, Anal, p. 140.

Geng, P., Mei, S.Y., Zhang, J., Chen, P.L., Zhang, Y.Y., Yan, Q.X., 2019. Study on seismic performance of shield tunnels under combined effect of axial force and bending moment in the longitudinal direction. Tunn. Undergr. Space Technol. 91, 13.

Geng, P., Wang, Q., Guo, X., Zeng, G., Chen, C., He, C., 2020. Pull-out test of lonogitudinal joints of shield tunnel. China J. Highw. Transp. 33, 124–134 (in Chinese).

Guo, W., Feng, K., Zhou, Y., Lu, X., Qi, M., He, C., Xiao, M., 2023. Experimental and numerical investigation on the shear behavior and damage mechanism of segmental joint under compression-shear load. Tunn. Undergr. Space Technol. 139.

Guo, R., He, C., Su, Z., Peng, Z., 2011. Study of Shearing Mechanical Properties of Segment Joints of Shield Tunnels. Modern Tunnelling Technology 48, 72–77.

Han, X., Oreste, P., Ye, F., 2023a. The buoyancy of the tunnel segmental lining in the surrounding filling material and its effects on the concrete stress state. Geotech. Geol. Eng. 41, 741–758.

Han, X., Oreste, P., Ye, F., 2023b. The contribution of the bolting system to the shear stiffness of circumferential joints in tunnel segmental linings. Comput. Geotech. 162, 1–21.

Han, X., Oreste, P., Ye, F., 2023c. The important role of stiffnesses values of circular joints on the stress state developed in the tunnel segmental lining. Geomech. Geophys. Geo-Energy Geo-Resour. 9, 1–32.

He, Y., Yang, Z., Liu, X., Ding, W., 2021. Theoretical solution for failure mechanism of circumferential joint of shield tunnel segment connected using diagonal bolts. Tunnel Constr. 41, 933–945 (in Chinese).

Huang, Z., Fu, H., Chen, W., Zhang, J., Huang, H., 2018. Damage detection and quantitative analysis of shield tunnel structure. Autom. Constr. 94, 303–316.

Li, D., Chen, Z., Yang, Z., 2011. Test and analysis of shear performance of Circumferential joint of segment ring. Undergr. Eng. Tunnels 15–17 (in Chinese).

Li, Y., Tannant, D.D., Pang, J., Su, G., 2021. Experimental and analytical investigation of the shear resistance of a rock joint held by a fully-grouted bolt and subject to large deformations. Transp, Geotech, p. 31.

Li, X.J., Zhou, X.Z., Hong, B.C., Zhu, H.H., 2019. Experimental and analytical study on longitudinal bending behavior of shield tunnel subjected to longitudinal axial forces. Tunn. Undergr. Space Technol. 86, 128–137.

Liao, S.M., Peng, F.L., Shen, S.L., 2008. Analysis of shearing effect on tunnel induced by load transfer along longitudinal direction. Tunn. Undergr. Space Technol. 23, 421–430.

Liu, J., Shi, C., Wang, Z., Lei, M., Zhao, D., Cao, C., 2021b. Damage mechanism modelling of shield tunnel with longitudinal differential deformation based on elastoplastic damage model. Tunn. Undergr. Space Technol. 113.

Liu, D.J., Wang, F., Hu, Q.F., Huang, H.W., Zuo, J.P., Tian, C., Zhang, D.M., 2020. Structural responses and treatments of shield tunnel due to leakage: A case study. Tunn. Undergr. Space Technol. 103, 18.
Liu, D.J., Tian, C., Wang, F., Hu, Q.F., Zuo, J.P., 2021a. Longitudinal structural deformation mechanism of shield tunnel linings considering shearing dislocation of circumferential joints. Comput. Geotech. 139, 15.
Maekawa, K., Qureshi, J., 1997. Stress transfer across interfaces in reinforced concrete due to aggregate interlock and dowel action. J. Materials. Conc. Struct 34, 159–172.
Nie, W., Guo, W., Ma, S., Zhao, Z., 2020. Numerical Modelling of Fully Grouted Rockbolts Subjected to Shear Load. Rock Mech. Rock Eng. 53, 2493–2503.
Oreste, P.P., Cravero, M., 2008. An analysis of the action of dowels on the stabilization of rock blocks on underground excavation walls. Rock Mech. Rock Eng. 41, 835–868.
Oreste, P., Spagnoli, G., 2021. A probabilistic approach for the evaluation of the stabilizing forces of fully grouted bolts. Transp, Geotech, p. 28.
Poli, S.D., Prisco, M.D., Gambarova, P.G., 1992. Shear response, deformations, and subgrade stiffness of a dowel bar embedded in concrete. ACI Structural Jourrnal 665–675.
Qiu, Y., Hu, X., Walton, G., He, C., He, C., Woody, J.u., J.,, 2021. Full scale tests and a progressive failure model to simulate full mechanical behavior of concrete tunnel segmental lining joints. Tunn. Undergr. Space Technol. 110.
Shi, C., Cao, C., Lei, M., Peng, L., Ai, H., 2016. Effects of lateral unloading on the mechanical and deformation performance of shield tunnel segment joints. Tunn. Undergr. Space Technol. 51, 175–188.
Shi, C.H., Wang, Z.X., Gong, C.J., Liu, J.W., Peng, Z., Cao, C.Y., 2022. Prediction of the additional structural response of segmental tunnel linings induced by asymmetric jack thrusts. Tunn. Undergr. Space Technol. 124, 19.
Shiba, Y., Kawashima, K., Obinata, N., Kano, T., 1988. An evaluation method of longitudinal stiffness of shield tunnel linings for application to seismic response analyses. J. Jpn. Soc. Civ. Eng 319–327 (in Japanese).
Soroushian, P., Obaseki, K., Rojas, M.C., 1987a. Bearing strength and stiffness of concrete under reinforcing bars. ACI Materials Journal 84, 179–184.
Soroushian, P., Obaseki, K., Rojas, M.C., 1987b. Behavior of Bars in Dowel Action against Concrete Cover. ACI Materials Journal 84, 179–184.
Vintzēleou, E.N., Tassios, T.P., 1986. Mathematical models for dowel action under monotonic and cyclic conditions. Magazine of Concrete Research 38, 13–22.
Wu, H.N., Shen, S.L., Liao, S.M., Yin, Z.Y., 2015. Longitudinal structural modelling of shield tunnels considering shearing dislocation between segmental rings. Tunn. Undergr. Space Technol. 50, 317–323.
Xu, G., He, C., Lu, D., Wang, S., 2019. The influence of longitudinal crack on mechanical behavior of shield tunnel lining in soft-hard composite strata. Thin-Walled Struct. 144.
Yang, Y., Zhou, B., Xie, X., Liu, C., 2017. Characteristics and causes of cracking and damage of shield tunnel segmented lining in construction stage – a case study in Shanghai soft soil. Eur. J. Environ. Civ. Eng. 22, s213–s227.
Yin, W., Lu, H., Yuan, J., Huang, B., 2022. Mechanical characteristics of dowel bar-concrete interaction: based on substructure experiment. International Journal of Pavement Engineering 23, 2392–2404.
Zhang, D., Liu, J., Li, B., Zhong, Y., 2020a. Shearing behavior of circumferential joints with oblique bolts in large diameter shield tunnel. China J. Highw. Transp. 33, 142–153 (in Chinese).
Zhang, L., Feng, K., Li, M., He, C., Xiao, M., Zhang, Z., 2020b. Characteristic analysis on the compression-bending capacity of segmental joint based on the investigated joint parameters. Tunn. Undergr. Space Technol. 102.
Zhang, W., Qi, J., Zhang, G., Niu, R., Zhang, C., He, L., Lyu, J., 2022. Full-scale experimental study on failure characteristics of the key segment in shield tunnel with super-large cross-section. Tunn. Undergr. Space Technol. 129.
Zuo, L., Zhang, J., Feng, K., Yang, W., Zhang, L., He, C., 2022. Experimental study on Inter-ring joint shearing characteristics of gas transmission shield tunnel with bent bolt and tenon. Tunn. Undergr. Space Technol. 130.